TITLE:

Location bias contributes to functionally selective responses of biased CXCR3 agonists

AUTHORS:

Dylan Scott Eiger[1]

Noelia Boldizsar[2]

Christopher Cole Honeycutt[2]

Julia Gardner[2]

Stephen Kirchner[3,4]

Chloe Hicks[2]

Issac Choi[5]

Uyen Pham[1]

Kevin Zheng[2]

Anmol Warman[2]

Jeffrey Smith[6-10]

Jennifer Zhang[3]

Sudarshan Rajagopal[1,5,*,ǫ]

[*] = corresponding author

[ǫ] = lead contact

AFFILIATIONS:

[1]Department of Biochemistry, Duke University, Durham, NC, 27710, USA

[2]Trinity College, Duke University, Durham, NC, 27710, USA

[3]Department of Dermatology, Duke University, Durham, NC, 27707, USA

[4]Department of Molecular Genetics and Microbiology, Duke University, Durham, NC, 27707, USA

[5]Department of Medicine, Duke University, Durham, NC, 27710, USA

[6]Department of Dermatology, Massachusetts General Hospital, Boston, MA, 02114, USA

[7]Department of Dermatology, Brigham and Women's Hospital, Boston, MA, 02115, USA

[8]Department of Dermatology, Beth Israel Deaconess Medical Center, Boston, MA, 02215, USA

[9]Dermatology Program, Boston Children's Hospital, Boston, MA, 02115, USA

[10]Harvard Medical School, Boston, MA, 02115, USA

CORRESPONDENCE

sudarshan.rajagopal@duke.edu

SUMMARY

Some G protein-coupled receptor (GPCR) ligands act as “biased agonists” which preferentially activate specific signaling transducers over others. Although GPCRs are primarily found at the plasma membrane, GPCRs can traffic to and signal from many subcellular compartments. Here, we determine that differential subcellular signaling contributes to the biased signaling generated by three endogenous ligands of the chemokine GPCR CXCR3. The signaling profile of CXCR3 changed as it trafficked from the plasma membrane to endosomes in a ligand-specific manner. Endosomal signaling was critical for biased activation of G proteins, β-arrestins, and ERK1/2. In CD8+ T cells, the chemokines promoted unique transcriptional responses predicted to regulate inflammatory pathways. In a mouse model of contact hypersensitivity, β-arrestin-biased CXCR3-mediated inflammation was dependent on receptor internalization. Our work demonstrates that differential subcellular signaling is critical to the overall biased response observed at CXCR3, which has important implications for drugs targeting chemokine receptors and other GPCRs.

KEYWORDS: beta-arrestin, G protein-coupled receptor, biased agonism, chemokine, CXCR3, endosome, MAP kinase, location bias, inflammation, bioluminescence resonance energy transfer

INTRODUCTION

G Protein-Coupled Receptors (GPCRs) are the largest superfamily of membrane proteins, accounting for about 5% of all genes encoded in the human genome (Zhang et al., 2006), and are the target of approximately 35% of all Food and Drug Administration-approved drugs (Sriram and Insel, 2018). GPCR signaling is mediated by effectors including G proteins, GPCR kinases (GRKs), and β-arrestins, which modulate the activity of a variety of signaling pathways, like those mediated by cyclic adenosine monophosphate (cAMP), extracellular-signal-regulated kinase (ERK), and protein kinase A (PKA) (Wootten et al., 2018). GPCR signaling is implicated in a wide range of normal physiologic processes (Kamal and Jockers, 2011), and the dysregulation of GPCRs is associated with various pathologies (Zalewska et al., 2014). Ligand:receptor interactions at GPCRs can preferentially activate certain signaling pathways over others in a ligand-, receptor- or cell-dependent manner, a phenomenon referred to as 'biased agonism' or 'functional selectivity' (Smith et al., 2018a). There is a desire to develop *biased agonists* that selectively activate some signaling pathways over others to generate beneficial physiologic responses while reducing off-target effects. However, the molecular mechanisms underlying biased signaling remain unclear.

Adding to this complexity has been the realization that GPCRs can signal from subcellular compartments with altered signaling profiles, resulting in 'location bias' as an additional mechanism of signaling specificity (Calebiro et al., 2009; Irannejad et al., 2017; Tsvetanova and von Zastrow, 2014). GPCRs can undergo receptor-mediated endocytosis and be recycled back to the plasma membrane, targeted to lysosomes for degradation, or trafficked to specific subcellular locations (Irannejad et al., 2015). It was previously thought that GPCR internalization abolished signaling by limiting the membrane-accessible GPCR pool or via receptor degradation (Irannejad and von Zastrow, 2014). However, it was later appreciated that GPCRs can activate G protein- and β-arrestin-mediated signaling pathways from both the plasma membrane and endosomes (Ferrandon et al., 2009; Irannejad et al., 2013; Kotowski et al., 2011), and other subcellular compartments, like the Golgi apparatus and endoplasmic reticulum (ER) (Mohammad Nezhady et al., 2020). Internalized GPCR signaling is an enticing therapeutic target with potential to broaden our ability to manipulate GPCR-mediated physiological processes and disease states (Jensen et al., 2017; Jimenez-Vargas et al., 2021; Thomsen et al., 2018). However, it is unclear to what extent subcellular signaling contributes to the overall biased signaling exhibited by GPCRs.

The physiologic significance of location bias is difficult to determine as most biased agonists are synthetic ligands. However, chemokine receptors (CKRs) represent a subfamily of GPCRs consisting of approximately 20 receptors and 50 endogenous ligands that interact to regulate many cellular functions like chemotaxis, angiogenesis, and neuromodulation (Eiger et al., 2021). CKRs are promiscuous in that some receptors bind multiple ligands, and some ligands bind multiple receptors. For example, CXCR3 is a CKR with three endogenous ligands, CXCL9, CXCL10, and CXCL11, and is expressed primarily on effector T cells (Colvin et al., 2006; Colvin et al., 2004; Groom and Luster, 2011). CXCR3 signaling, like many other CKRs, is primarily mediated by both Gαi- and β-arrestin-dependent pathways (Smith et al., 2017). Previous work has shown that CXCL11 is relatively β-arrestin biased compared to CXCL9 and CXCL10, and each chemokine demonstrates distinct abilities to promote receptor-mediated endocytosis (Colvin et al., 2004; Smith et al., 2017; Smith et al., 2018b).

With its biased signaling and internalization and central role in regulating T cell biology, we studied CXCR3 and its endogenous ligands to determine how ligand bias extends beyond the plasma membrane to the endosome, with implications for sustained, differential signaling at specific subcellular compartments. We demonstrate that the CXCR3 ligands activate G proteins and β-arrestins differently at the endosome compared to the plasma membrane. Furthermore, downstream signaling responses, like kinase activation and cellular transcription, are differentially regulated by the endogenous ligands in a manner dependent on receptor internalization. We determine that the chemokines differentially modulate transcriptional pathways related to inflammation in primary CD8+ T cells, and demonstrate that internalization is required to fully potentiate the inflammatory response in a mouse model of contact hypersensitivity. We demonstrate how biased GPCR signaling can change as the receptor traffics to a subcellular compartment with important physiological effects, and also highlight how a significant proportion of GPCR functional selectivity is dependent on sustained signaling following receptor internalization.

RESULTS

CXCR3 chemokines promote different amounts of β-arrestin-dependent receptor internalization

We first determined if the biased chemokines of CXCR3 promoted different amounts of receptor-mediated internalization in HEK293 cells. Using bioluminescence resonance energy transfer (BRET), we

monitored a luciferase-tagged CXCR3 as it traffics to endosomes with an FYVE domain-tagged mVenus, or away from the plasma membrane using a Myrpalm-tagged mVenus. Consistent with previous studies, the chemokines promoted different degrees of receptor-mediated endocytosis with CXCL11 being the most efficacious ligand **(Figure 1A)** (Colvin et al., 2004; Meiser et al., 2008). β-arrestins are known to interact with a variety of effector proteins, including those involved in endocytosis (Claing et al., 2001; Goodman et al., 1996; Laporte et al., 1999; Lefkowitz and Shenoy, 2005; McDonald et al., 1999). To determine the role β-arrestins play in receptor internalization at CXCR3, we studied CXCR3 internalization in β-arrestin 1/2 CRISPR KO cells (Alvarez-Curto et al., 2016; Luttrell et al., 2018). Internalization was abrogated in the absence of β-arrestin 1 and 2 and reintroduction of β-arrestin 1 and/or β-arrestin 2 rescued CXCR3 internalization following stimulation with CXCL10 and CXCL11, but not CXCL9 **(Figure 1B)**. Using confocal microscopy, we similarly observed an increase in receptor internalization upon rescue with β-arrestin 1 or β-arrestin 2 following stimulation with CXCL10 and CXCL11 **(Figure 1C)**. Together, these data demonstrate that the CXCL10 and CXCL11 promote CXCR3 internalization in a β-arrestin-dependent manner.

Biased G protein activation depends on receptor location

To determine how CXCR3 activates G proteins at the plasma membrane and endosomes, we used a location specific BRET biosensor to detect GTP-bound Gαi as a measure of G protein activation (Johnston et al., 2008; Maziarz et al., 2020b) **(Figure 2A and 2B)**. At the plasma membrane, CXCL11 promoted the most G protein activation followed by CXCL10 and lastly CXCL9 **(Figure 2C)**, consistent with previous reports (Berchiche and Sakmar, 2016; Smith et al., 2017). All CXCR3 endogenous ligands promoted G protein activation at the endosome **(Figure 2D)**. The amount of G protein activation was different than that observed at the plasma membrane; specifically, CXCL10 and CXCL11 had nearly identical G protein activation at the endosome but different amounts at the plasma membrane. Furthermore, CXCL11-induced G protein activation decreased in the endosome compared to the plasma membrane, while those of CXCL9 and CXCL10 did not change **(Figure 2E-G)**, demonstrating that the impact of receptor location on G protein signaling is ligand-specific.

Gαi family members are myristolated, which localizes these proteins to the plasma membrane (Oldham and Hamm, 2008). We then tested if the relative change in endosomal G protein activation could be explained by different amounts of *total* G protein present in the endosomes. To do this, we developed a split nanoluciferase

assay to determine the *absolute* amount of Gαi present in endosomes, irrespective of Gαi nucleotide status **(Figure 2H)**. We found that Gαi rapidly translocated to the endosome following stimulation with the CXCR3 ligands, and the total amount of endosomal G protein mirrored a chemokine's ability to induce receptor internalization **(Figure 2I and 2J)**. Therefore, although similar amounts of endosomal G protein activation were observed following treatment with CXCL10 and CXCL11, when considering the absolute amount of endosomal G protein, CXCL11 promoted relatively *less* G protein activation than CXCL10. These data demonstrate location bias in G protein activation, with different levels of G protein activation at the plasma membrane compared to the endosome depending on the agonist.

CXCR3-mediated cAMP inhibition is differentially dependent on receptor internalization

We next studied the effect of inhibiting endocytosis on the intracellular accumulation of cAMP. While Gαs family members activate adenylyl cyclase (AC) to produce cAMP, Gαi family members inhibit AC. We utilized an exchange protein activated by cAMP (EPAC)-based BRET biosensor for cAMP that is ubiquitously expressed in cells (Masuho et al., 2015) **(Figure 3A)**. Prior to activation of the endogenous Gαs-coupled β2-adrenergic receptor (β2AR), HEK293 cells were preincubated with the CXCR3 ligands, allowing us to measure Gαi activity **(Figure 3A)**. To inhibit receptor-mediated internalization, we overexpressed a dominant-negative mutant of the GTPase Dynamin (Dynamin K44A), which is required for release of clathrin-coated vesicles from the plasma membrane (Damke et al., 1994). Using confocal microscopy, we confirmed that Dynamin K44A inhibited the translocation of membrane-bound CXCR3-GFP:β-arrestin 2-RFP complexes into endosomes **(Supplemental Figure 1A)**.

Chemokine inhibition of cAMP production mirrored Gαi nucleotide exchange, where CXCL11 and CXCL10 are significantly more potent and efficacious agonists than CXCL9 **(Figure 3B)**. Expression of Dynamin K44A reduced inhibition of cAMP production following stimulation with CXCL10 and CXCL11, but not CXCL9, reflecting a biased decrease in Gαi-coupled activity **(Figure 3C)**. CXCL10 and CXCL11 both demonstrated a ~40% decrease in cAMP inhibition when receptor internalization was inhibited, even though the chemokines were able to promote different amounts of total receptor internalization **(Figure 3D-3I)**. cAMP gradients can exist in micro or nanodomains within the cell, and endosomal cAMP production can be critical for nuclear translocation of effectors like PKA (Calebiro and Maiellaro, 2014; Musheshe et al., 2018; Peng et al., 2021). Using an EPAC

BRET biosensor localized to the nucleus, we found that the pattern of cAMP inhibition was nearly identical to that measured globally **(Supplemental Figure 1B-1J)**. These data demonstrate that receptor internalization is critical to the biased regulation of second messengers across subcellular compartments.

Biased ligands of CXCR3 promote differential patterns of β-arrestin 2 recruitment and conformation at the plasma membrane and the endosome

We next determined if the location-dependent functional selectivity observed in G protein signaling extended to β-arrestins. Consistent with previous studies, CXCL11 induced the most β-arrestin 2 recruitment to the plasma membrane, followed by CXCL10 and CXCL9 **(Figure 4A and 4B)** (Smith et al., 2017). While CXCL11 promoted robust and sustained β-arrestin 2 recruitment to endosomes, CXCL10 only weakly and transiently recruited β-arrestin 2, while CXCL9 showed no detectable endosomal recruitment **(Figure 4C-4D)**. GPCR affinity for β-arrestins can be classified as "Class A" GPCRs, which form transient complexes with β-arrestins, while "Class B" GPCRs form tight and long-lived complexes with β-arrestins (Jean-Charles et al., 2017; Oakley et al., 2000). CXCL9 and CXCL10 promote CXCR3 to behave like a "Class A" GPCR while CXCL11 promotes "Class B" behavior, a phenomenon previously described at other GPCRs (Janetzko et al., 2021; Rajagopal et al., 2013).

Recent research demonstrated that distinct conformations of β-arrestin mediate specific signaling events like GPCR desensitization, internalization, and effector scaffolding (Cahill et al., 2017; Coffa et al., 2011; Eichel et al., 2018; Latorraca et al., 2018). We developed an assay to quantify β-arrestin 2 conformation at specific cellular locations based on a previously described intramolecular fluorescent arsenical hairpin (FlAsH) BRET assay (Lee et al., 2016). This modified "complex FlAsH" assay takes advantage of a split nanoluciferase-coupled with FlAsH BRET **(Figure 4E and 4H)**, and provides a readout of β-arrestin 2 conformation at specific subcellular locations. We assessed the conformational status of β-arrestin 2 using two previously validated FlAsH constructs, FlAsH 4 and FlAsH 5, which demonstrate preserved β-arrestin recruitment to GPCRs (Lee et al., 2016). β-arrestin activation is associated with a ~20º rotation between its N- and C-domains (Shukla et al., 2013). Given the common location of the BRET acceptor on the β-arrestin 2 C-domain in the FlAsH 4 and FlAsH 5 constructs, these sensors serve as readouts of β-arrestin interdomain twist (Chen et al., 2018). We found that the biased ligands of CXCR3 display markedly distinct patterns of FlAsH conformational signatures at both the plasma membrane and the endosome, suggesting that bias in β-arrestin 2 conformation is different at specific

subcellular locations **(Figure 4F-4G and 4I-4J)**. While CXCL9 and CXCL10 recruited β-arrestin 2 to the plasma membrane, both chemokines did not induce significant change in β-arrestin 2 conformation at this location. CXCL11-induced distinct FlAsH signatures from CXCL9 and CXCL10 at the plasma membrane (**Figure 4F-4G)**. At the endosome, CXCL10 and CXCL11 induced significant but different changes in β-arrestin 2 conformation while CXCL9 demonstrated no change in conformation, consistent with its inability to recruit β-arrestin 2 to endosomes (**Figure 4I-4J)**. While the β-arrestin 2 conformation demonstrated an increase in BRET signal at the plasma membrane, we observed a decrease in BRET signal at the endosome, suggesting that β-arrestin 2 adopts a different conformation at the endosome compared to the plasma membrane. Not only do the chemokines differentially recruit β-arrestin 2 to the plasma membrane and the endosome, but the conformation of β-arrestin 2 is uniquely dependent on both agonist and location, consistent with location bias in β-arrestin activity between agonists.

Biased signaling profiles of the chemokines changes as the receptor traffics to endosomes

Biased agonism at GPCRs is commonly assessed in terms of the relative activation between G proteins and β-arrestins, and we summarized the above findings using bias plots **(Figure 4K-4L)** (Gregory et al., 2010; Rajagopal et al., 2011). Bias plots allow for simultaneous assessment of relative activity between two assays, and the best fit lines obtained for each chemokine can assess relative bias across the ligands. At the plasma membrane we observed that CXCL11 is slightly β-arrestin-biased compared to CXCL10. CXCL9 demonstrated a similar profile to CXCL11, but with partial agonist activity. At the endosome, CXCL11 demonstrated a relative decrease in G protein activation while still effectively coupling to β-arrestin. Conversely, CXCL9 and CXCL10 demonstrated a significant increase in relative G protein activation and simultaneous decrease in coupling to β-arrestin. Together, the relative β-arrestin-biased nature of CXCL11 and the G protein-biased nature of CXCL10 at the plasma membrane were increased in the endosome. CXCL9 acts as a partial β-arrestin biased agonist at the plasma membrane, but becomes significantly more G protein-biased in the endosome **(Supplemental Figure 2).**

CXCR3 signaling from endosomes differentially contributes to cytoplasmic and nuclear ERK activation

We next investigated the activation of the mitogen-activated protein kinase (MAPK) pathway through ERK 1/2 phosphorylation (pERK), a common GPCR signaling pathway (Grundmann et al., 2018; Luttrell et al., 2018). Using Western blotting of pERK from whole cell lysates, we observed significant increases in pERK by CXCL10 and CXCL11, and relatively less activation by CXCL9 at 5 minutes **(Figure 5A)**. Upon expression of Dynamin K44A, CXCL9-induced pERK was unchanged, while CXCL10 and CXCL11 demonstrated reduced pERK levels; however, this effect was not statistically significant **(Figure 5B)**. Similar findings across the chemokines were observed at 30 minutes, and pERK levels declined back to baseline at 60 minutes **(Supplemental Figure 3A)**.

To more accurately assess ERK 1/2 activation in different subcellular locations, we generated a BRET-based biosensor of the previously developed extracellular signal-regulated kinase activity reporter (EKAR) biosensor which reports on ERK kinase activity (Harvey et al., 2008) **(Supplemental Figure 3B)**. This biosensor can be localized to the nucleus or cytoplasm to allow for detection of ERK activity in different subcellular compartments **(Supplemental Figure 3C and 3D)**. Consistent with our immunoblots, we observed biased activation of cytoplasmic ERK by the chemokines **(Figure 5C-5E)**. Dynamin K44A partially abrogated cytoplasmic ERK activity at CXCL10 and CXCL11, but not CXCL9 **(Figure 5F)**. In contrast, we detected no measurable nuclear ERK activity with CXCL9 treatment, but substantial nuclear ERK activity with CXCL10 and CXCL11. Dynamin K44A expression led to near complete abrogation of nuclear ERK activity by both CXCL10 and CXCL11 **(Figure 5G-5J)**. These findings suggest that CXCR3 internalization is necessary for activation of nuclear ERK, while CXCR3 internalization contributes to, but is not required for, cytoplasmic ERK activation. Furthermore, while CXCL9 promotes cytoplasmic ERK activity, it does not promote measurable nuclear ERK activation.

Biased agonists are differentially dependent on internalization for transcriptional regulation

Previous studies have shown that certain transcriptional responses are dependent on sustained GPCR signaling from endosomes (Tsvetanova et al., 2015; Tsvetanova and von Zastrow, 2014). Notably, CXCL9, CXCL10, and CXCL11 have also previously been shown to differentially activate transcriptional reporters (Smith et al., 2017). To determine the contribution of CXCR3 signaling from endosomes to the transcriptional response, we studied the chemokine-induced activation of two transcriptional reporters, the serum response element

(SRE), which responds to ternary complex factor (TCF)-dependent MAPK/ERK signaling, and serum response factor response element (SRF-RE), which is a mutant form of SRE that responds to TCF-independent signaling pathways like RhoA (Hill et al., 1995). Consistent with previous work, CXCL11 promoted the most transcriptional activity at both reporters, followed by CXCL10 and CXCL9 in HEK293 cells **(Figure 6A and 6C)**. Overexpression of Dynamin K44A significantly decreased CXCL11-mediated transcriptional activity, but had no significant effect on CXCL9- and CXCL10-mediated transcriptional activity. Inhibition of endocytosis led to a 50% decrease in CXCL11-induced transcriptional activation, which was significantly greater than that observed at CXCL9 and CXCL10 **(Figure 6B and 6D)**. Interestingly, although CXCL10 promoted nuclear ERK activation in an endocytosis-dependent manner, inhibition of endocytosis did not impact CXCL10 activation of SRE to the same extent as CXCL11. These data suggest that CXCL10 and CXCL11 regulate transcriptional activation of this promoter element through different mechanisms, where CXCL11 demonstrates greater relative dependence on receptor internalization. Importantly, inhibition of endocytosis significantly decreased the degree of bias observed between the chemokines, demonstrating the critical role internalization plays in GPCR functional selectivity.

Chemokine-induced transcriptional responses in CD8+ T cells reveal differential activation of inflammatory pathways

CXCR3 is primarily found in blood, bone marrow, and lymphoid tissues, specifically on Th1-type CD4+ T cells and effector CD8+ T cells (Groom and Luster, 2011). To study the biased transcriptional regulation at CXCR3 in a more physiologically relevant cell type, the transcriptional response of primary, activated, CD8+ human T-cells expressing endogenous amounts of CXCR3 stimulated with the chemokines was characterized by RNA Sequencing (RNA-Seq) **(Supplemental Figure 4A and 4B)**. We observed significant changes in global transcriptional activation, detecting approximately 48000 transcripts, 887 of which varied by chemokine treatment **(Figure 4E).** There was a high degree of replicability between biological replicates **(Supplemental Figures 4C-4F)**. The majority of differentially expressed genes (DEGs) increased in transcript level following chemokine treatment **(Supplemental Figure 4G-4K)**. CXCL11 demonstrated the largest number of DEGs, consistent with our data in HEK293 cells **(Figure 6F)**. Importantly, CXCL10 and CXCL11 demonstrate transcriptional profiles where the majority of DEGs were only found following treatment with each specific chemokine, rather than being shared across chemokines. These data contrast with that observed at CXCL9 – although it promoted significant

transcriptional activation, approximately 66% of CXCL9-induced DEGs were shared with CXCL10 and or CXCL11 **(Figure 6F)**.

We next analyzed the DEGs by Gene Set Enrichment Analysis (GSEA) using the Molecular Signatures Database (mSigDB) (Subramanian et al., 2005). GSEA identified differentially activated biological pathways and processes corresponding to predefined mSigDB gene sets. Compared to vehicle control, the chemokines induce biased activation of pathways including interleukin JAK/STAT signaling, Myc targets, and TNF-α/NF-κB, among others. Comparison of DEGs between chemokines revealed differential activation of 8 gene sets between CXCL9 and CXCL10, 24 between CXCL9 and CXCL11, and 11 gene sets between CXCL10 and CXCL11 **(Figure 6G-6I)**. Among them, several were proinflammatory including TNF-α/NF-κB, IL6/JAK/STAT3, MYC, mTORC1, and IFNγ related pathways. CXCL11 was enriched in pathways related to the transcription factor MYC and apoptosis, suggesting that CXCL11 plays a role in regulating T-cell growth (Schmidt, 1999). In contrast, CXCL10 shows enrichment in cytokine related pathways (JAK/STAT, INFγ), complement, and inflammatory responses, suggesting that CXCL10 may promote a pro-inflammatory T-cell phenotype. These findings highlight the lack of conserved transcriptional response across the chemokines, demonstrating the physiologic role of sustained signaling from endosomes in biased regulation of inflammatory pathways.

CXCR3 internalization contributes to potentiation of inflammation in a murine model of contact hypersensitivity

We previously showed in a murine model of allergic contact hypersensitivity (CHS) that a synthetic β-arrestin-biased CXCR3 agonist, VUF10661, potentiates inflammation through increased recruitment of CD8+ T cells in a β-arrestin 2-dependent manner (Smith et al., 2018b). To determine if this response requires sustained CXCR3 signaling from endosomes, we inhibited receptor-mediated internalization in this CHS model. Following sensitization, CHS was elicited through application of the allergen dinitrofluorobenzene (DNFB) or vehicle control to the ears of the mice with concomitant administration of VUF10661 and a pharmacologic inhibitor of Dynamin, Dyngo 4a (Eichel et al., 2016; Jensen et al., 2017; McCluskey et al., 2013). Ear thickness was measured as a marker of inflammation **(Figure 7A)**. Previous work showed that VUF10661 in the absence of DNFB does not illicit an inflammatory response (Smith et al., 2018b) and we observed similar findings with Dyngo 4a

(Supplemental Figure 5). Therefore, any increase in ear thickness was primarily due to modulated DNFB-induced inflammation, and not directly from the compounds tested.

Following DNFB sensitization and treatment, mice treated with VUF10661 demonstrated a 60% increase in ear thickness over control **(Figure 7C)**. This effect was decreased in mice that received concomitant administration of Dyngo 4a and VUF10661 compared to control, with only a 20% increase in ear thickness. These results are consistent with the conclusion that sustained CXCR3 signaling from endosomes is required for maximal potentiation of the inflammatory response. Together, these data demonstrate the *in vivo* role of subcellular GPCR signaling in modulating inflammation.

DISCUSSION

Our findings are synthesized in a working model of how location bias by CXCR3 chemokine agonists promote functionally selective responses with distinct effects on inflammation **(Figure 7C).** At the plasma membrane, the chemokines demonstrate biased engagement of G proteins and β-arrestins leading to different amounts of β-arrestin-dependent receptor-mediated endocytosis. In the endosomes, we observed relative changes in signaling across all chemokines, where CXCL11 became more β-arrestin-biased while CXCL9 and CXCL10 demonstrated enhanced coupling to G proteins. CXCR3 signaling from the plasma membrane and endosome both contributed to the cytosolic activation of ERK1/2; however, only CXCL10 and CXCL11 activated nuclear ERK1/2 in a manner almost entirely dependent on signaling from endosomes. This functionally selective and location-dependent signaling converged to differentially regulate transcription in both HEK293 cells and primary CD8+ T cells, with differential effects on genes that play important roles in inflammation. Lastly, we found that inhibiting endocytosis in a CXCR3-mediated CHS model in mice significantly decreased inflammation. Together these findings suggest a physiologically important role for location bias in CXCR3 signaling that contributes to the inflammatory response.

It was previously believed that ligand:receptor interactions in the CKR family were redundant (Mantovani, 1999). Considerable evidence has challenged this notion and demonstrated that a significant proportion of CKR signaling is indeed specific to particular ligand:receptor combinations (Corbisier et al., 2015; Mikucki et al., 2015; Rabin et al., 1999; Rajagopal et al., 2013). Here we show that the functional selectivity observed at CKRs persists beyond the plasma membrane into subcellular compartments like the endosome. Additionally, location bias is

critical for some, but not all, ligands, to their functional selectivity. Given that GPCRs are known to translocate to locations like the Golgi apparatus, it is possible that trafficking to other cellular compartments may demonstrate signaling patterns different than those observed in this study (Eichel and von Zastrow, 2018; Mohammad Nezhady et al., 2020; Pavlos and Friedman, 2017). Additionally, some GPCRs simultaneously exist on multiple membrane bound structures, like the nucleus and mitochondria (Mohammad Nezhady *et al.*, 2020), enabling for even greater signaling diversity for membrane permeable ligands.

While all of the chemokines couple CXCR3 to β-arrestin 2 at the plasma membrane, only CXCL10 and CXCL11 were able to translocate β-arrestin to endosomes, albeit to different extents. The biased chemokines also promoted unique β-arrestin conformations at the plasma membrane which persisted as the receptor trafficked to the endosome. Because β-arrestin conformation is directly related to function, it is likely these conformational differences contribute to biased receptor signaling (Lee *et al.*, 2016). β-arrestin can engage the GPCR core (core conformation) which is associated with G protein desensitization; however, it can also bind to the GPCR C-terminal tail (tail conformation), which is associated with receptor internalization and effector scaffolding (Cahill *et al.*, 2017; Kumari et al., 2016). There is also evidence of GPCR:G protein:β-arrestin "megaplexes" which allow for sustained G protein signaling, with simultaneous engagement of β-arrestin in the tail conformation (Nguyen et al., 2019; Thomsen et al., 2016). We observed a relative decrease in G protein signaling in endosomes following treatment with CXCL11 but not with CXCL10. It is possible that CXCL10 promotes β-arrestin to adopt a tail conformation that drives receptor internalization without further desensitization of G protein signaling. Although CXCL11 promotes greater amounts of total endosomal β-arrestin, it is possible that a relatively larger proportion of this β-arrestin adopts a core conformation.

Our assessments of downstream signaling demonstrate the functional diversity that can be obtained through a single GPCR using biased agonists. Biased MAPK activation observed across the CXCR3 chemokines was dependent on subcellular location. We observed significant differences in transcriptional activation that directly correspond with the ability of a ligand to activate ERK, consistent with prior studies (Whitmarsh et al., 1995). Although overexpression of Dynamin K44A eliminated nuclear ERK activation at CXCL10 and CXCL11, we only observed a significant decrease in transcriptional activity with CXCL11 treatment. It is possible that CXCL10 and CXCL11 activate certain promoter elements through different mechanisms. This is consistent with

recent reports demonstrating that some membrane bound GPCRs can activate MAPKs via multiple mechanism, such as translocation of Gβγ proteins to the Golgi apparatus (Khater et al., 2021).

Our findings highlight the critical role of ligand bias and location bias in GPCR signaling, which were further demonstrated in the diverse transcriptional responses observed in primary CD8+ T cells and a murine model of CHS. Previous work at the Neurokinin 1 receptor (NK_1R) showed that signaling from endosomes was critical for prolonged nociception (Jensen et al., 2017). A NK_1R antagonist which trafficked with the receptor to endosomes demonstrated sustained GPCR antagonism and heightened antinociception, revealing the clinical utility of GPCR targeted therapeutics that function at multiple cellular locations (Jensen et al., 2017). We found that GPCRs can adopt multiple different signaling profiles and trafficking patterns, simply by changing the ligand used to activate the receptor. We demonstrated the potential utility of developing pharmaceutical drugs that not only activate the receptor in a biased fashion, but also target the receptor to one or multiple subcellular compartments. Given that our work was conducted at CXCR3, it is important to understand how temporospatial functional selectivity contributes to disease pathologies at other CKRs and GPCRs in order to develop more targeted, efficacious, and safer therapeutics. Because biased agonism has recently been observed at other receptor superfamilies like receptor tyrosine kinases (Karl et al., 2020), this work has important implications in harnessing the functional selectivity of chemokine receptors, GPCRs, and other transmembrane receptors at and beyond the plasma membrane.

ACKNOWLEDGEMENTS

We thank R.J. Lefkowitz (Duke University, USA) for guidance, mentorship, and thoughtful feedback throughout this work; N. Nazo for laboratory assistance. Funding: This work was supported by T32GM007171 (D.S.E.), the Duke Medical Scientist Training Program (D.S.E.), AHA 20PRE35120592 (D.S.E.), 1R01GM122798 (S.R.), K08HL114643 (S.R.), Burroughs Wellcome Career Award for Medical Scientists (S.R.), Duke University Dean's Summer Research Fellowship (N.B., C.C.H).

AUTHOR CONTRIBUTIONS

Conceptualization, D.S.E., S.R.; Methodology, D.S.E., S.R.; Investigation, D.S.E., N.B., C.C.H., J.G., S.K., C.H., I.C., U.P., K.Z., A.W.; Writing - Original Draft, D.S.E., N.B., C.C.H., J.G, C.H., K.Z., A.W.; Writing - Reviewing & Editing, D.S.E., N.B., C.C.H., J.G., S.K., J.S.S, J.Z., and S.R.; Visualization, D.S.E and S.R.; Supervision and Funding Acquisition, J.Z. and S.R.

DECLARATION OF INTERESTS

The authors declare no competing interests.

INCLUSION AND DIVERSITY

One or more of the authors of this paper self-identifies as an underrepresented ethnic minority in science. While citing references scientifically relevant for this work, we also actively worked to promote gender balance in our references list.

MAIN FIGURE TITLES AND LEGENDS

Figure 1: CXCR3 receptor-mediated internalization is differentially regulated by biased chemokines and dependent on β-arrestin. (A) CXCR3 trafficking to early endosomes using the BRET acceptor 2x-Fyve-mVenus or away from the plasma membrane using Myrpalm-mVenus in HEK293 cells. **(B)** CXCR3 trafficking away from the plasma membrane using Myrpalm-mVenus in β-arrestin 1/2 knock out cells. Data are normalized to maximum signal and are the mean ± SEM, n=4. *P < .05 by one-way or two-way ANOVA. For **(A)**, post-hoc testing was conducted between ligands within each BRET acceptor and for **(B)** post-hoc testing was conducted between pcDNA 3.1 and every other transfection condition within a ligand. (**C)** Confocal microscopy images of β-arrestin 1/2 knock out cells transfected with CXCR3-mCerulean and either pcDNA 3.1, β-arrestin 1, or β-arrestin 2 following the listed treatment for 45 minutes. Images are representative of three replicates.

Figure 2: CXCR3 G protein signaling changes as the receptor traffics away from the plasma membrane to the endosome. Schematic representation of the location-specific BRET-based GTP-Gαi sensor. Following G protein activation, the GTP bound Gαi-mVenus will interact with the peptide KB-1753-NLuc, which selectively binds GTP-bound Gαi 1-3, to produce a BRET signal. The peptide is localized to the **(A)** plasma membrane or the **(B)** endosome. Agonist dose-dependent formation of GTP-Gαi at the **(C)** plasma membrane or **(D)** endosome in HEK293 cells. **(E-G)** Data for each ligand at the plasma membrane and endosome are presented according to ligand identity. Data for figures **(C-G)** are normalized to CXCL11-induced GTP-Gαi at the plasma membrane. **(H)** Schematic representation of the split nanoluciferase assay detecting total endosomal Gαi irrespective of Gαi nucleotide status. **(I)** Agonist dose-dependent and **(J)** kinetic data of Gαi-LgBit recruitment to endosomes tagged with 2xFyve-SmBit. Data are the mean ± SEM, n=3-6. * denotes statistically significant differences between E_{max} of ligands.

Figure 3: Maximal Gαi mediated cAMP inhibition at CXCR3 is dependent on receptor endocytosis. (A) Schematic representation of the cAMP sensor experimental design (Masuho *et al.*, 2015). Agonist dose-dependent inhibition of isoproterenol-induced cAMP production by the chemokines in HEK293 cells with concurrent transfection of **(B)** pcDNA 3.1 or **(C)** Dynamin K44A to inhibit internalization. **(D to F)** Kinetic data

and **(G to I)** agonist dose-dependent of cAMP inhibition levels in HEK293 cells treated with CXCL9, CXCL10 and CXCL11, respectively. Data are the mean ± SEM, n=5. * denotes statistically significant differences between E_{max} for dose response data of pcDNA 3.1 versus Dynamin K44A transfection conditions at each ligand. See Figure S1 for similar data on nuclear cAMP.

Figure 4: CXCR3 demonstrates biased β-arrestin 2 recruitment and conformation between chemokine agonists at the plasma membrane and endosome. Kinetic data and quantification of area-under-the-curve (AUC) of β-arrestin-2 recruitment to the **(A and B)** plasma membrane or **(C and D)** endosome following 100nM chemokine stimulation of CXCR3. **(E)** Schematic of complex FlAsH assay to detect β-arrestin 2 conformation. Cells express LgBit-CAAX and a modified SmBit-β-arrestin 2 complex FlAsH construct. Upon complex FlAsH recruitment to the plasma membrane, complementation between the LgBit and SmBit creates a functional nanoluciferase protein which can undergo BRET with the intramolecular tetracysteine motif. **(F and G)** Complex FlAsH 4 and 5 plasma membrane BRET data for CXCR3 treated with chemokines. **(H)** Schematic of complex FlAsH assay, similar to Figure 4E, to detect β-arrestin 2 conformation at the endosome, using 2x-Fyve-LgBit. **(I and J)** Complex FlAsH 4 and 5 endosomal BRET data for CXCR3 treated with chemokines. **(K and L)** Bias plots demonstrating relative G protein activation and β-arrestin 2 recruitment at the plasma membrane and endosome across the chemokines. Arrows highlight the change in best fit lines between CXCL10 and CXCL11. For β-arrestin 2 recruitment assays, data are the mean ± SEM, n=3. * denotes statistically significant differences between AUC between different chemokines. For complex FlAsH assays, data are the mean ± SEM, n=3-5. *P<.05 by one-way ANOVA with Tukey's post-hoc testing conducted between ligands within each FlAsH construct. $^{\#}$P<.05 by a one-sample *t*-test is listed beneath each chemokine to determine if the Net BRET value was non-zero. See also Figure S2.

Figure 5: CXCR3 internalization is required for biased cytoplasmic and nuclear ERK1/2 activation. (A) Representative western blot and **(B)** quantification of ERK1/2 phosphorylation following 5 minutes of stimulation with vehicle control or chemokine with transfection of pcDNA 3.1 or Dynamin K44A. Data are the mean ± SEM, n=5 and are normalized to CXCL11 and pcDNA 3.1. Kinetic data and quantification of AUC of ERK activity using the **(C-F)** cytoplasmic and **(G-J)** nuclear ERK BRET biosensors following chemokine treatment with transfection

of pcDNA 3.1 or Dynamin K44A. Data are the mean ± SEM, n=3-4. *P<.05 using a two-way ANOVA analysis with comparisons made between pcDNA 3.1 or Dynamin K44A within a ligand. See also Figure S3.

Figure 6: Biased transcriptional regulation at CXCR3 is dependent on receptor trafficking to endosomes. Transcriptional activity of CXCR3-expressing HEK293 cells transfected with a **(A)** serum response element (SRE) or **(C)** serum response factor response element (SRF-RE) luciferase reporter and either pcDNA 3.1 or Dynamin K44A. Percent of **(B)** SRE or **(D)** SRF-RE signal retained when overexpressing Dynamin K44A. For luciferase reporter assays, data are the mean ± SEM, n=4. *P<.05 using a two-way ANOVA analysis with comparisons made between pcDNA 3.1 or Dynamin K44A within a ligand. A one-way ANOVA with Tukey's post-hoc testing was conducted for **(B)** and **(D)**. **(E)** Heat map of differentially expressed genes (DEGs) in primary CD8+ T-cells. **(F)** Venn diagram of DEGs compared to vehicle treatment. **(G-I)** Gene set enrichment analysis of differentially regulated pathways between chemokines. Listed pathways are statistically significant at P < .05, however, select pathways are labelled as TRUE if the False Discovery Rate (FDR) is < 0.25 and FALSE if the FDR is > 0.25. See also Figure S4 for additional informatics analysis of CXCR3 transcriptomics.

Figure 7: Receptor internalization is required for maximum CXCR3-mediated inflammation. (A) Experimental design of the dinitrofluorobenzene (DNFB)-induced contact hypersensitivity mouse model. Mice are sensitized with DNFB on their back, followed by induction of inflammation with DNFB or vehicle control on the ears four days later. This is followed by treatment with VUF10661 with or without Dyngo 4a at 0, 24 hours, and 48 hours. **(B)** Ear thickness following DNFB elicitation and application of VUF10661 (50nM) with or without Dyngo 4a (50nM). Data are presented as the VUF10661-induced increase in ear thickness over control (DMSO or Dyngo 4a alone – see Figure S5 for changes in ear thickness associated with control treatments). Data are means ± SEM of 7-10 mice per treatment group. *P < .05 using a two-way ANOVA analysis. **(C)** Working model demonstrating how location bias contributes to functionally selective cellular signaling and inflammatory responses at CXCR3.

STAR Methods

RESOURCE AVAILABILITY

Lead Contact

Further information and requests for resources and reagents should be directed to and will be fulfilled by the lead contact, Sudarshan Rajagopal (Sudarshan.rajagopal@duke.edu).

Materials Availability

All plasmids generated in this study will be distributed upon request.

Data and Code Availability

RNA-seq data have been deposited at GEO and are publicly available as of the date of publication. Accession numbers are listed in the key resources table. All data reported in this paper will be shared by the lead contact upon request.

EXPERIMENTAL MODEL AND SUBJECT DETAILS

Bacterial strains

XL-10 Gold ultracompetent E. coli (Agilent) were used to express all constructs used in this manuscript.

Cell Lines

Human Embryonic Kidney (HEK293, β-arrestin 1/2 knockout) cells were grown in minimum essential media (MEM) supplemented with 10% fetal bovine serum (FBS) and 1% penicillin/streptomycin at 37°C and 5% CO2. β-arrestin ½ CRISPR/Cas9 KO HEK293 cells were provided by Asuka Inoue and validated as previously described (Alvarez-Curto *et al*., 2016). CD8+ T cells were cultured in RPMI 1640 supplemented with 10% FBS and 1% penicillin/streptomycin at 37°C and 5% CO2.

Animal Studies

All animal procedures performed in this study were in agreement with the Guide for the Care and Use of Laboratory Animals of the National Institutes of Health. Animals were housed in Duke University's GSRBII and protocols for use were approved by Duke University's Institutional Animal Care and Use Committee. All animals were housed under the Duke University protocol number A104-20-05. Female WT C57BL/6 (Charles River) mice were bred and maintained under specific pathogen–free conditions in accredited animal facilities at the Duke University under the animal protocol. Because the ear inflammation in this CHS model causes mice to scratch and gnaw at their ears, excessive scratching can produce artificially large increases in ear thickness. To minimize this phenomenon, female mice were chosen as they tend to be less aggressive than male mice and can additionally be socially housed (Jirkof et al., 2020; Olsson and Westlund, 2007).

METHOD DETAILS

Generation of Constructs

Construct cloning was performed using conventional techniques such as restriction enzyme/ligation methods. Linkers between the fluorescent proteins or luciferases and the cDNAs for receptors, transducers, or other proteins were flexible and ranged between 2 and 18 amino acids. Dr. Kirill Martemyanov provided the EPAC plasmid which was used to clone the nuclear specific EPAC cAMP sensors. EKAR FRET ERK1/2 biosensors previously published (Harvey et al., 2008) were used to generate BRET versions of these sensors by removing the N-terminal mCerulean through restriction digest and inserting a nanoluciferase.

Cell Culture and Transfection

For BRET and luminescence-based assays, HEK293 cells were transiently transfected with an optimized calcium phosphate protocol as previously described unless otherwise indicated (Pack et al., 2018). In the calcium phosphate transfection method, cell culture media was replaced 30 minutes prior to transfection. Plasmid constructs were suspended in water to a final volume of 90µL. 10 µL of 2.5 M calcium chloride was added to the plasmid constructs and mixed. 100 µL of 2x HEPES-buffered saline solution (10mM D-Glucose, 40mM HEPES,

10 mM potassium chloride, 270 mM sodium chloride, 1.5 mM disodium hydrogen phosphate dihydrate) was added to the solution, allowed to incubate for two minutes, and subsequently added to the cells.

For BRET biosensors for compartmentalized ERK activity and cAMP levels, transcriptional reporter assays, and confocal microscopy, cells were transiently transfected using polyethylenimine (PEI). In the PEI transfection method, cell culture media was replaced 30 minutes prior to transfection. Plasmid constructs were suspended in Opti-MEM (GIBCO) to a final volume of 100 µL and, in a separate tube, PEI at a concentration of 1 mg/mL was added to Opti-MEM to a final volume of 100 µL. For experiments in this manuscript, 3 µL of PEI was used per 1µg of plasmid DNA. After 5 minutes, the 100 µL PEI solution was added to the 100 µL DNA solution, gently mixed, and allowed to incubate at room temperature for 10-15 minutes, after which the mixture was added to the cells.

BRET and Split Luciferase Assays

For all BRET and Split Luciferase assays, HEK293 cells seeded in 6 well plates were transiently transfected using the calcium phosphate method described previously unless otherwise indicated.

To determine G protein nucleotide status, we took advantage of and modified a previously described two component BRET sensor (Maziarz et al., 2020a). The first component of the biosensor consists of a plasma membrane targeting domain anchor, a synthetic peptide KB-1753 that selectively and reversibly binds to GTP-bound Gαi (Gαi 1-3) (Johnston et al., 2008), and a nanoluciferase BRET donor. By altering the identity of the lipid anchor, the sensor can be used to detect G protein activation at different cellular locations. Specifically, the GTP-bound Gαi sensor located at the plasma membrane (Mas-KB1753-NLuc) has a myristic attachment sequence (mas) targeting sequence (MGSSKSKTSNS) (Maziarz et al., 2020a). We generated a GTP-bound Gαi sensor with a 2x-Fyve targeting sequence from the hepatocyte growth factor-regulated tyrosine kinase substrate to target it to the endosome (2xFyve-KB1753-NLuc). When co-expressed with Gαi-mVenus, the sensor will bind to the active Gαi subunit following guanine nucleotide exchange of GDP for GTP and produce a BRET signal.

G protein localization to endosomes irrespective of nucleotide status was detected using wild-type CXCR3, Gαi-LgBit, and 2xFyve-SmBit. The role of β-arrestin in receptor internalization was assessed using wild-type CXCR3 tagged with a C-terminal RLuc2, Myrpalm tagged mVenus or 2x-Fyve tagged mVenus, and rescue

of β-arrestin 1, β-arrestin 2, both β-arrestin isoforms, or pcDNA 3.1 control. β-arrestin recruitment was assessed using wild-type CXCR3, SmBit-β-arrestin 2, and either 2xFyve-LgBit to detect β-arrestin 2 at endosomes or LgBit-CAAX to detect β-arrestin 2 at the plasma membrane.

Location-specific BRET-biosensors of downstream signaling (EPAC and EKAR) were transfected using PEI. The EPAC-based BRET biosensor (Masuho et al., 2015) consists of an N-terminal nanoluciferase and two C-terminal Venus constructs. Following production of cAMP by the endogenously expressed Gαs-coupled β2-adrenergic receptor (β2AR), the BRET biosensor will bind cAMP and undergo a conformational change which leads to a decrease in BRET efficiency. The EKAR biosensor consists of a target substrate that, following phosphorylation by activated pERK, binds to a phosphorylation binding domain, causing a conformational change in the biosensor and subsequent change in BRET efficiency.

Twenty-four hours after transfection, cells were washed with phosphate buffered saline, collected with trypsin, and plated onto a clear bottom, white-walled, 96 well plate at 50,000-100,000 cells/well in clear minimum essential medium supplemented with 2% FBS, 1% penicillin/streptomycin, 10mM HEPES, 1x GlutaMax, and 1x Antibiotic-Antimycotic (Gibco). The next day, the media were removed, and cells were incubated at room temperature with 80 µL of 3µM coelenterazine h in Hanks' balanced salt solution (HBSS) (Gibco) supplemented with 5mM HEPES for 5-10 minutes before adding ligand at the appropriate concentration. For BRET assays assessing CXCR3 internalization, HEK293 cells were stimulated with 100nM of each chemokine and the data shown are average Net BRET ratios calculated between 25 and 30 minutes following stimulation.

For EPAC assays, 100 nM chemokine and coelenterazine h were added simultaneously and allowed to incubate for 15 minutes prior to the addition of 1 µM isoproterenol to promote cAMP formation. For split luciferase assays to assess Gαi-Lgbit and SmBit-β-arrestin 2 trafficking, as well as BRET EKAR and EPAC assays, three initial reads were taken prior to the addition of ligand to quantify baseline luminescence or BRET before adding ligand. Plates were read with a BioTek Synergy Neo2 plate reader set at 37°C. All readings were performed using a kinetic protocol.

BRET plates were read using a 480 nm wavelength filter and 530 nm wavelength filter. BRET ratios were calculated by dividing the 530 nm acceptor signal by the 480 nm donor signal. Net BRET ratios were calculated by subtracting the vehicle BRET ratio from the ligand stimulated BRET ratio. Split luciferase plates were read

without a wavelength specific filter. Baseline luminescence was subtracted from each read following ligand addition to calculate a change in luminescence after ligand stimulation and then normalized to vehicle treatment.

Complex Intramolecular Fluorescent Arsenical Hairpin (FlAsH) BRET of β-arrestin 2

HEK293 cells seeded in six-well plates were transiently transfected with wild-type CXCR3, SmBit-tagged FlAsH 4 or 5, and either 2xFyve-LgBit or LgBit-CAAX using the calcium phosphate transfection protocol. In this complex FlAsH assay, CCPGCC tetracysteine sequences were inserted into a β-arrestin 2 construct following amino acids 225 in FlAsH 4 and 263 in FlAsH 5 (Lee et al., 2016). These tetracysteine motifs are capable of binding the organoarsenic compound FlAsH-EDT_2. The original FlAsH constructs have an N-terminal luciferase which, in the complex FlAsH assay, is replaced with a SmBit (Lee et al., 2016). When the β-arrestin 2 complex FlAsH construct is recruited to one of the tagged intracellular locations, complementation occurs between the LgBit and SmBit, creating a functional nanoluciferase protein. The produced luminescent signal (~460nm) can undergo resonance energy transfer (RET) with the intramolecular FlAsH-EDT_2, which serves as an acceptor moiety to produce a BRET signal (~530nm). The efficiency of RET depends on the distance and conformation between the split nanoluciferase and FlAsH-EDT_2. Thus, this assay provides a readout of β-arrestin 2 conformation as measured between the N-terminus and two different locations on the β-arrestin 2 C-domain at specific subcellular locations.

Twenty-four hours after transfection, cells were plated onto clear-bottomed, rat-tail collagen coated, white-walled, Costar 96-well plates at 100,000 cells/well in minimum essential medium (Gibco) supplemented with 10% fetal bovine serum and 1% penicillin-streptomycin (P/S). The following day, cells were washed with 50 µL of HBSS (Gibco). 100 µL of 2.5 µM FlAsH-EDT_2 in HBSS was added for arsenical labeling, and cells were incubated in the dark at 37ºC for 45 minutes. FlAsH-EDT_2 was aspirated, and the cells were washed with 130 µL of 250 µM 2,3 dimercaptopropanol (BAL) wash buffer. Cells were then incubated at room temperature with 80 µL of 3 µM coelenterazine h in Hanks' balanced salt solution (Gibco) supplemented with 20mM HEPES for 5-10 minutes. Following a 5-minute incubation in 37°C, three prereads were taken to measure baseline BRET ratios. Chemokine was then added to 100 nM final concentration. Plates were read with a BioTek Synergy Neo2 using a 480 nm wavelength filter and 530 nm wavelength filter. Readings were performed using a kinetic protocol. BRET ratios were calculated by dividing the 530 nm signal by 480 nm signal. Net BRET values were calculated

as described above by averaging six consecutive BRET values and normalizing to vehicle control. Net BRET values of β-arrestin 2 conformation using the membrane tag LgBit-CAAX were calculated at 5 minutes following ligand stimulation, while Net BRET values using the endosome tag 2xFyve-LgBit were calculated at 20 minutes following ligand stimulation.

Immunoblotting

Immunoblotting was performed as described previously (Smith et al., 2018b). HEK293 cells seeded in 12 well plates were transiently transfected with wild-type CXCR3 and either pcDNA 3.1 or Dynamin K44A using the calcium phosphate transfection method. 24 hours after transfection, cells were serum starved in minimum essential medium supplemented with 0.01% bovine serum albumin (BSA) and 1% penicillin/streptomycin for 16 hours. The cells were then stimulated with 100nM chemokine or vehicle control for 5, 30, or 60 minutes, washed with ice cold PBS, and lysed in ice cold RIPA buffer supplemented with phosphatase and protease inhibitors (Phos-STOP (Roche), cOmplete EDTA free (Sigma)). The samples were rotated at 4°C for forty-five minutes and cleared of insoluble debris by centrifugation at 17,000g at 4°C for 15 minutes, after which the supernatant was collected. Protein was resolved on SDS-10% polyacrylamide gels, transferred to nitrocellulose membranes, and immunoblotted with the indicated primary antibody overnight at 4°C. phospho-ERK (Cell Signaling Technology, #9106) and total ERK (Millipore Sigma, #06-182) antibodies were used to assess ERK activation. Horseradish peroxidase-conjugated anti-rabbit-IgG or anti-mouse-IgG were used as secondary antibodies. The nitrocellulose membranes were imaged by SuperSignal enhanced chemiluminescent substrate (Thermo Fisher) using a ChemiDoc MP Imaging System (Bio-Rad). Following detection of pERK signal, nitrocellulose membranes were stripped and reblotted for tERK signal. Relative ERK activation was calculated by dividing the intensity of pERK by tERK and comparing this ratio for a specific experimental condition to that of vehicle treatment.

Transcriptional Reporter Assays – SRE and SRE-SF

HEK293 cells seeded in 6 well plates were transiently transfected with SRE or SRF-RE reporter plasmids, wild type CXCR3, and either pcDNA 3.1 or Dynamin K44A using the PEI transfection method. Twenty-four hours after transfection, cells were washed with PBS, collected with trypsin, and plated onto a clear bottom, white-walled, 96 well plate at 50,000-100,000 cells/well and starved overnight in serum-free minimum-essential media

(Gibco) supplemented with 1% penicillin/streptomycin. The cells were then incubated with 100 nM CXCL9, CXCL10, or CXCL11 for six hours. The wells were aspirated and then incubated with 1.6mM luciferin in Hanks' balanced salt solution (Gibco) supplemented with 20mM HEPES for ten minutes. Luminescence was quantified at 480nm using a BioTek Synergy Neo2 plate reader set at 37°C. Transcriptional activity was quantified by calculating the fold-change in luminescence of ligand-treated cells from vehicle-treated cells. The fold-change was then normalized to maximum signal.

Confocal Microscopy

HEK293 cells were plated on rat-tail-collagen-coated 35 mm glass bottomed dishes (MatTek Corporation, Ashland, MA) and transiently transfected using PEI with the listed constructs. Forty-eight hours following transfection, the cells were washed once with PBS and then serum starved for one hour. The cells were subsequently treated with a control of serum free media or the listed chemokine at 100nM or VUF10661 at 10μM for forty-five minutes at 37°C. Following stimulation, the cells were washed once with HBSS and fixed at room temperature in the dark in a 6% formaldehyde solution for 20 minutes. Cells were subsequently washed four times with PBS and then imaged. The cells were imaged with a Zeiss CSU-X1 spinning disk confocal microscope using the corresponding lasers for GFP (480nm excitation), RFP (561nm excitation), and mCerulean (433nm excitation). Images were analyzed using ImageJ (NIH, Bethesda, MD).

RNA sequencing

Primary, negatively selected, CD8+ T cells were obtained commercially (*Precision for Medicine*, Bethesda, MD). T cells were cultured in RPMI medium 1640 containing 10% FBS, 1% penicillin/streptomycin at 37°C and 5% CO_2. Prior to stimulation, T-cells were activated and expanded using anti-CD3 and anti-CD28 magnetic beads, and subsequently recultured without magnetic beads, as previous work has shown that this protocol increases T-cell count and surface expression of CXCR3 (Nakajima et al., 2002). Specifically, T cells were activated using CD3/CD28 T-cell Dynabeads (Thermo Fischer) at a 1:1 bead:cell ratio for three days and then cultured without Dynabeads for three more days in fresh media. Cells were starved for four hours in RPMI medium 1640 containing 0.01% BSA and 1% penicillin/streptomycin and subsequently stimulated with vehicle or chemokine for 2 hours. Total RNA was extracted using the RNeasy Plus RNA Extraction Kit (Qiagen). RNA sequencing was

conducted by Novogene Co. (Beijing, China). For heat maps, genes with an adjusted p-value <0.05 were considered as differentially expressed. For UpSet plots, genes with an adjusted p-value <0.05 and |log2(Foldchange)| > 0.3 are shown. For Volcano plots, genes with an adjusted p-value <0.05 and |log2(Foldchange)| > 0.4 are labelled. Gene set enrichment analysis was performed to determine whether chemokine treatments generated significant differences for *a priori* defined set of genes from the Molecular Signatures database (https://www.gsea-msigdb.org/gsea/index.jsp).

Quantitative Polymerase Chain Reaction (qPCR)

RNA isolated from peripheral blood mononuclear cells were reverse transcribed into complementary DNA (cDNA) using the iScript cDNA synthesis kit (Bio-Rad) according to the manufacturer's instructions. cDNA was analyzed using iTaq Universal SYBR Green Supermix (Bio-Rad) using the CXCR3 primers 5' GCCATGGTCCTTGAGGTGAG 3' and 5' GGAGGTACAGCACGAGTCAC 3' and 18s rRNA primers forward 5' GTAACCCGTTGAACCCCATT 3' and 5' CCATCCAATCGGTAGTAGCG 3'. cDNA levels were measured using an Applied Biosystems 7300 Real-Time PCR system. PCR was performed first through polymerase activation and denaturation at 95ºC for 30 seconds. cDNA then underwent 40 cycles of denaturation at 95ºC for 15 seconds, and annealed, extension, and reading at 60ºC for 60 seconds. Data are expressed as fold change ($2^{-\Delta\Delta Ct}$) of each target gene compared to 18s rRNA, and then normalized to No Treatment control.

DNFB Contact Hypersensitivity Murine Model

Seven-week-old mice were split into groups of 7-10 mice when sensitized. Animals were randomly assigned to treatment groups and investigators were blinded to pharmacologic treatments. Mice were initially sensitized by topical application of 50µL of 0.5% DNFB (Sigma Aldrich) in a 4:1 acetone:olive oil solution on their shaved back. Four days later, they were challenged on their ears with 10µL of 0.3% DNFB with or without Dyngo 4a (50 µM). 4, 24, and 48 hours later, 10µL of either vehicle control, VUF10661 (50 µM), Dyngo 4a (50 µM), or VUF10661 and Dyngo 4a (both at 50 µM) dissolved in a 72:18:10 acetone:olive oil:DMSO solution was applied to the ear by a blinded investigator. Ear thickness was measured at the listed time points with an engineer's micrometer (Standard Gage). To determine if Dyngo 4a had any effect on ear thickness in the absence of DNFB, we

797 performed the above experiment in the absence of DNFB or VUF10661 and measured mouse ear thickness until
798 96 hours after initial Dyngo 4a treatment.
799
800 **CXCR3 Ligands**
801 Recombinant Human CXCL9, CXCL10, and CXCL11 (PeproTech) were diluted according to the manufacturer's
802 specifications, and aliquots were stored at −80°C until needed for use. VUF10661 (Sigma-Aldrich) was
803 reconstituted in dimethyl sulfoxide (DMSO) and were stored at −20°C in a desiccator cabinet.
804
805 **QUANTIFICATION AND STATISTICAL ANALYSIS**
806
807 **Statistical analyses**
808 Dose-response curves were fitted to a log agonist versus stimulus with three parameters (span, baseline, and
809 EC50), with the minimum baseline corrected to zero using Prism 9.0 (GraphPad, San Diego, CA). Statistical
810 tests were performed using a one or two-way ANOVA followed by Tukey's multiple comparison's test when
811 comparing treatment conditions. When comparing ligands or treatment conditions in concentration-response
812 assays or time-response assays, a two-way ANOVA of ligand and concentration or ligand and AUC, respectively,
813 was conducted. If a significant interaction effect was observed ($P < 0.05$), then comparative two-way ANOVAs
814 between individual experimental conditions were performed. Further details of statistical analysis and replicates
815 are included in the figure legends. Lines represent the mean, and error bars signify the SEM, unless otherwise
816 noted.
817
818 **Bias Plots**
819 To generate bias plots, raw or normalized dose response data for G protein activation and β-arrestin 2 are plotted
820 for each chemokine at a specific location. We defined G protein activation as the ability of the chemokine to
821 induce Gαi nucleotide exchange relative to the total amount of Gαi present at that location. Best fit lines were
822 then plotted for each chemokine.
823

824 **KEY RESOURCES TABLE**

REAGENT OR RESOURCE	SOURCE	IDENTIFIER
Antibodies		
Donkey polyclonal anti-rabbit IgG peroxidase conjugated	Rockland	Cat#611-7302; RRID:AB_219747
Sheep polyclonal anti-mouse IgG peroxidase conjugated	Rockland	Cat#610-603-002; RRID:AB_219694
Mouse monoclonal anti-phospho-p44/42 MAPK 1/2 (ERK1/2) (Thr202/Tyr204)	Cell Signaling Technologies	Cat#9106; RRID:AB_331768
Rabbit polyclonal anti-MAPK 1/2 (ERK1/2)	Millipore Sigma	Cat#06-182; RRID:AB_310068
Bacterial Strains		
XL10-Gold Ultracompetent E. Coli	Agilent	Cat#200315
Chemicals, peptides, and recombinant proteins		
Recombinant Human CXCL9	Peprotech	Cat#300-26
Recombinant Human CXCL10	Peprotech	Cat#300-12
Recombinant Human CXCL11	Peprotech	Cat#300-46
VUF10661	Sigma-Aldrich	Cat#SML0803
Dyngo 4a	Abcam	Cat#AB120689
1-Fluoro-2,4-dinitrobenzene	Sigma-Aldrich	Cat#D1529
GlutaMax	Gibco	Cat#35050061
Antibiotic-Antimycotic	Gibco	Cat#15240062
FlAsH-EDT2	Santa Cruz Biotechnology	Cat#sc-363644
Coelenterazine h	Cayman Chemical	Cat#16894
Coelenterazine h	NanoLight Technology	Cat#301
QuikChange Lightning Site-Directed Mutagenesis Kit	Agilent	Cat#210518
PhosSTOP	Sigma-Aldrich	Cat#4906845001
cOmplete Protease Inhibitor Cocktail	Sigma-Aldrich	Cat#11697498001
SuperSignal West Pico PLUS Chemiluminescent Substrate	Thermo Fischer Scientific	Cat#34580
Dynabead Human T-Activator CD3/CD28 for T Cell Expansion and Activation	Thermo Fischer Scientific	Cat#11131D
D-Luciferin	Goldbio	Cat#LUCK-100
Isoproterenol	Sigma-Aldrich	Cat#I6504
Critical commercial assays		
iScript cDNA Synthesis Kit	Bio-Rad	Cat#1708890
RNeasy Plus Kit	Qiagen	Cat#74134
iTaq Universal SYBR Green Supermix	Bio-Rad	Cat#1725121
Deposited Data		
CD8+ T-Cell RNA-seq	This paper; GEO	GSE192679
Experimental Models: Cell Lines		
Human: HEK293	ATCC	Cat#CRL-1573;RRID:CVCL_0045
Human: 293T β-arrestin 1/2 Knock Out	Asuka Inoue	(Alvarez-Curto *et al.*, 2016)

Human: CD8+ T-Cells, Negatively Selected	Precision for Medicine	N/A
Experimental Models: Organisms/strains		
C57BL/6 Female Mice	Charles River	Cat#C57BL/6NCrl; RRID:IMSR_CRL:027
Oligonucleotides		
CXCR3 fwd primer GCCATGGTCCTTGAGGTGAG	Sigma-Aldrich	N/A
CXCR3 rev primer GGAGGTACAGCACGAGTCAC	Sigma-Aldrich	N/A
18s fwd primer GTAACCCGTTGAACCCCATT	Sigma-Aldrich	N/A
18s rev primer CCATCCAATCGGTAGTAGCG	Sigma-Aldrich	N/A
Recombinant DNA		
pcDNA3.1_CXCR3	Rajagopal Lab	N/A
pcDNA3.1_CXCR3-RLuc2	Rajagopal Lab	N/A
pcDNA3.1_Myrpalm-mVenus	Rajagopal Lab (Smith *et al.*, 2017)	N/A
pcDNA3.1_2x-Fyve-mvenus	Rajagopal Lab (Smith *et al.*, 2017)	N/A
β-arrestin 1	Lefkowitz Lab	N/A
β-arrestin 2	Lefkowitz Lab	N/A
pcDNA3.1_Mas-KB-1753-Nluc	Garcia-Marcos Lab (Maziarz et al. 2020)	N/A
pcDNA3.1_2xFyve-KB-1753-nLuc	This work	N/A
pcDNA3.1_Gαi-mVenus	Rajagopal Lab	N/A
Gαi1-LgBit	(Inoue et al., 2019)	N/A
pcDNA3.1_2xFyve-SmBit	This work	N/A
NLuc-EPAC-VV	Martemyanov Lab (Masuho *et al.*, 2015)	N/A
NLuc-EPAC-VV-NLS	This work	N/A
pBk-HA-1-DI-K44A	Lefkowitz Lab	N/A
SmBit-Barr2	Rajagopal Lab	N/A
pcDNA3.1_2xFyve-LgBit	This work	N/A
pcDNA3.1_SmBit-Barr2-FlAsH 4	This work	N/A
pcDNA3.1_SmBit-Barr2-FlAsH 5	This work	N/A
pcDNA3.1_LgBit-CAAX	This work	N/A
pcDNA3.1_Cyto-EKAR BRET Biosensor	This work	N/A
pcDNA3.1_Nuc-EKAR BRET Biosensor	This work	N/A
pGL4.33[*luc*2P/SRE/Hygro]	Promega	Cat#E1340
pGL4.34[*luc*2P/SRF-RE/Hygro]	Promega	Cat#PS087
pcDNA3.1_CXCR3-mCerulean	This work	N/A
pcDNA3.1_CXCR3-GFP	This work	N/A
β-arrestin 2-RFP	Marc Caron Lab	N/A
Software and algorithms		
GraphPad Prism	GraphPad Software	https://www.graphpad.com/scientific-software/prism/
ImageJ	(Schneider et al., 2012)	https://imagej.nih.gov/ij/

Adobe Illustrator	Adobe	https://www.adobe.com/
Excel	Microsoft	https://www.microsoft.com/en-us/microsoft-365/excel
ImageLab	Bio-Rad	https://www.bio-rad.com/en-us/product/image-lab-software
BioRender	BioRender	https://biorender.com/
Gene Set Enrichment Analysis	(Subramanian *et al.*, 2005)	https://www.gsea-msigdb.org/gsea/index.jsp

SUPPLEMENTAL FIGURE TITLES AND LEGENDS

Supplemental Figure 1: Gαi mediated cAMP inhibition at CXCR3 as measured using a nuclear localized cAMP sensor. Related to Figure 3.

(A) Confocal microscopy images of HEK293 cells transfected with CXCR3-GFP, β-arrestin 2-RFP (β-arr-2-RFP), and either pcDNA 3.1 or Dynamin K44A demonstrating successful inhibition of endocytosis with overexpression of Dynamin K44A. **(B)** Confocal and brightfield microscopy images of HEK293 cells transfected with a nuclear localized cAMP BRET biosensor (NLuc-EPAC-VV-NLS). Agonist dose-dependent inhibition of isoproterenol-induced nuclear cAMP production by the chemokine in HEK293 cells with concurrent transfection of **(C)** pcDNA 3.1 or **(D)** Dynamin K44A to inhibit internalization. **(E to G)** Kinetic data and **(H to J)** agonist dose-dependent inhibition of cAMP signal in HEK293 cells treated with chemokine. Data are the mean ± SEM, n = 5. * denotes statistically significant differences between E_{max} for dose response data of pcDNA 3.1 versus Dynamin K44A transfection conditions at each ligand.

Supplemental Figure 2: Plot of maximal G protein and β-arrestin signaling at different subcellular locations. Related to Figure 4. Plot of maximal G protein activation and β-arrestin 2 recruitment at the plasma membrane and endosome. All data are normalized to the values for CXCL11 at the plasma membrane. Gαi activation at the endosome was calculated by dividing the relative amount of endosomal Gαi-GTP by total endosomal Gαi.

Supplemental Figure 3: ERK activation at 30 and 60 minutes and premise of ERK biosensor. Related to Figure 5. (A) Representative immunoblot of ERK1/2 phosphorylation following 30 and 60 minutes of stimulation with vehicle control or 100nM of chemokine with transfection of pcDNA 3.1 or Dynamin K44A. **(B)** Schematic of the BRET based ERK biosensor (Harvey et al., 2008). The biosensor consists of an N-terminal nanoluciferase (NLuc), phosphobinding domain, flexible linker, ERK substrate peptide, ERK docking domain, and C-terminal mVenus. Following phosphorylation of the target peptide by activated ERK, the phosphobinding domain will complex with the phosphothreonine, bringing the NLuc and mVenus in close proximity to generate a BRET signal. **(C and D)** Confocal microscopy of the ERK biosensors targeted to the cytoplasm or the nucleus.

Supplemental Figure 4: Approach and source data for RNA-seq to assess transcription in CD8+ T cells. Related to Figure 6. (A) Schematic of experimental design of RNA-seq experiments on activated primary CD8+ T cells. T cells were cultured with anti-CD3/CD28 T-cell Dynabeads (Thermo Fisher) for three days and then three days without Dynabeads to induce T cell activation and expansion. T cells were serum starved and incubated with the listed treatment condition for 2 hours. RNA was then isolated and then processed for RNA sequencing. **(B)** Quantitative PCR (qPCR) of peripheral blood mononuclear cells to examine CXCR3 transcript levels following stimulation with anti-CD3/CD28 magnetic beads. Cells were cultured under five conditions: No stimulation, 2 days with magnetic beads (2d On), 2 days with magnetic beads followed by 2 days without magnetic beads (2d On + 2d Off), 3 days with magnetic beads (3d On), or 3 days with magnetic beads followed by 3 days without magnetic beads (3d On + 3d Off). Transcript levels were normalized using 18s rRNA, and then subsequently normalized to the No stimulation condition. Data are the mean ± SEM, n=3. **(C-F)** Venn diagram showing common transcripts identified across three replicates within each treatment group demonstrating high degrees of replicability between replicate samples. UpSet Plots demonstrating similarly or differentially **(G)** upregulated or **(H)** downregulated transcripts at a Log2(Fold Change) of >±0.3. The UpSet Plots demonstrate that the majority of differential gene expression observed in our data set is not shared between the chemokines. **(I-K)** Volcano plots comparing differentially expressed transcripts between the listed treatment condition and vehicle control. Labelled transcripts are statistically significant and demonstrate a Log2(Fold Change) of >±0.4.

Supplemental Figure 5: Dyngo 4a treatment alone does not illicit an inflammatory response. Related to Figure 7. Ear thickness following application of Dyngo 4a (50nM) or DMSO control in the absence of VUF10661 or DNFB to assess for a nonspecific effect of Dyngo 4a treatment. Mice were treated with listed treatments at 0 hours, 24 hours, and 48 hours**.** Data are means ± SEM of 5-6 mice per treatment group. *P<.05 using a two-way ANOVA analysis.

References

Alvarez-Curto, E., Inoue, A., Jenkins, L., Raihan, S.Z., Prihandoko, R., Tobin, A.B., and Milligan, G. (2016). Targeted Elimination of G Proteins and Arrestins Defines Their Specific Contributions to Both Intensity and Duration of G Protein-coupled Receptor Signaling. J Biol Chem *291*, 27147-27159. 10.1074/jbc.M116.754887.

Berchiche, Y.A., and Sakmar, T.P. (2016). CXC Chemokine Receptor 3 Alternative Splice Variants Selectively Activate Different Signaling Pathways. Mol Pharmacol *90*, 483-495. 10.1124/mol.116.105502.

Cahill, T.J., Thomsen, A.R., Tarrasch, J.T., Plouffe, B., Nguyen, A.H., Yang, F., Huang, L.Y., Kahsai, A.W., Bassoni, D.L., Gavino, B.J., et al. (2017). Distinct conformations of GPCR-β-arrestin complexes mediate desensitization, signaling, and endocytosis. Proc Natl Acad Sci U S A *114*, 2562-2567. 10.1073/pnas.1701529114.

Calebiro, D., and Maiellaro, I. (2014). cAMP signaling microdomains and their observation by optical methods. Front Cell Neurosci *8*, 350. 10.3389/fncel.2014.00350.

Calebiro, D., Nikolaev, V.O., Gagliani, M.C., de Filippis, T., Dees, C., Tacchetti, C., Persani, L., and Lohse, M.J. (2009). Persistent cAMP-signals triggered by internalized G-protein-coupled receptors. PLoS Biol *7*, e1000172. 10.1371/journal.pbio.1000172.

Chen, Q., Iverson, T.M., and Gurevich, V.V. (2018). Structural Basis of Arrestin-Dependent Signal Transduction. Trends Biochem Sci *43*, 412-423. 10.1016/j.tibs.2018.03.005.

Claing, A., Chen, W., Miller, W.E., Vitale, N., Moss, J., Premont, R.T., and Lefkowitz, R.J. (2001). beta-Arrestin-mediated ADP-ribosylation factor 6 activation and beta 2-adrenergic receptor endocytosis. J Biol Chem *276*, 42509-42513. 10.1074/jbc.M108399200.

Coffa, S., Breitman, M., Hanson, S.M., Callaway, K., Kook, S., Dalby, K.N., and Gurevich, V.V. (2011). The effect of arrestin conformation on the recruitment of c-Raf1, MEK1, and ERK1/2 activation. PLoS One *6*, e28723. 10.1371/journal.pone.0028723.

Colvin, R.A., Campanella, G.S., Manice, L.A., and Luster, A.D. (2006). CXCR3 requires tyrosine sulfation for ligand binding and a second extracellular loop arginine residue for ligand-induced chemotaxis. Mol Cell Biol *26*, 5838-5849. 10.1128/MCB.00556-06.

Colvin, R.A., Campanella, G.S., Sun, J., and Luster, A.D. (2004). Intracellular domains of CXCR3 that mediate CXCL9, CXCL10, and CXCL11 function. J Biol Chem *279*, 30219-30227. 10.1074/jbc.M403595200.

Corbisier, J., Galès, C., Huszagh, A., Parmentier, M., and Springael, J.Y. (2015). Biased signaling at chemokine receptors. J Biol Chem *290*, 9542-9554. 10.1074/jbc.M114.596098.

Damke, H., Baba, T., Warnock, D.E., and Schmid, S.L. (1994). Induction of mutant dynamin specifically blocks endocytic coated vesicle formation. J Cell Biol *127*, 915-934. 10.1083/jcb.127.4.915.

Eichel, K., Jullie, D., Barsi-Rhyne, B., Latorraca, N.R., Masureel, M., Sibarita, J.B., Dror, R.O., and von Zastrow, M. (2018). Catalytic activation of beta-arrestin by GPCRs. Nature *557*, 381-386. 10.1038/s41586-018-0079-1.

Eichel, K., Jullie, D., and von Zastrow, M. (2016). beta-Arrestin drives MAP kinase signalling from clathrin-coated structures after GPCR dissociation. Nat Cell Biol *18*, 303-310. 10.1038/ncb3307.

Eichel, K., and von Zastrow, M. (2018). Subcellular Organization of GPCR Signaling. Trends Pharmacol Sci *39*, 200-208. 10.1016/j.tips.2017.11.009.

Eiger, D.S., Boldizsar, N., Honeycutt, C.C., Gardner, J., and Rajagopal, S. (2021). Biased agonism at chemokine receptors. Cell Signal *78*, 109862. 10.1016/j.cellsig.2020.109862.

Ferrandon, S., Feinstein, T.N., Castro, M., Wang, B., Bouley, R., Potts, J.T., Gardella, T.J., and Vilardaga, J.P. (2009). Sustained cyclic AMP production by parathyroid hormone receptor endocytosis. Nat Chem Biol *5*, 734-742. 10.1038/nchembio.206.

Goodman, O.B., Jr., Krupnick, J.G., Santini, F., Gurevich, V.V., Penn, R.B., Gagnon, A.W., Keen, J.H., and Benovic, J.L. (1996). Beta-arrestin acts as a clathrin adaptor in endocytosis of the beta2-adrenergic receptor. Nature *383*, 447-450. 10.1038/383447a0.

Gregory, K.J., Hall, N.E., Tobin, A.B., Sexton, P.M., and Christopoulos, A. (2010). Identification of orthosteric and allosteric site mutations in M2 muscarinic acetylcholine receptors that contribute to ligand-selective signaling bias. J Biol Chem *285*, 7459-7474. 10.1074/jbc.M109.094011.

Groom, J.R., and Luster, A.D. (2011). CXCR3 in T cell function. Exp Cell Res *317*, 620-631. 10.1016/j.yexcr.2010.12.017.

Grundmann, M., Merten, N., Malfacini, D., Inoue, A., Preis, P., Simon, K., Ruttiger, N., Ziegler, N., Benkel, T., Schmitt, N.K., et al. (2018). Lack of beta-arrestin signaling in the absence of active G proteins. Nat Commun *9*, 341. 10.1038/s41467-017-02661-3.

Harvey, C.D., Ehrhardt, A.G., Cellurale, C., Zhong, H., Yasuda, R., Davis, R.J., and Svoboda, K. (2008). A genetically encoded fluorescent sensor of ERK activity. Proc Natl Acad Sci U S A *105*, 19264-19269. 10.1073/pnas.0804598105.

Hill, C.S., Wynne, J., and Treisman, R. (1995). The Rho family GTPases RhoA, Rac1, and CDC42Hs regulate transcriptional activation by SRF. Cell *81*, 1159-1170. 10.1016/s0092-8674(05)80020-0.

Inoue, A., Raimondi, F., Kadji, F.M.N., Singh, G., Kishi, T., Uwamizu, A., Ono, Y., Shinjo, Y., Ishida, S., Arang, N., et al. (2019). Illuminating G-Protein-Coupling Selectivity of GPCRs. Cell *177*, 1933-1947 e1925. 10.1016/j.cell.2019.04.044.

Irannejad, R., Pessino, V., Mika, D., Huang, B., Wedegaertner, P.B., Conti, M., and von Zastrow, M. (2017). Functional selectivity of GPCR-directed drug action through location bias. Nat Chem Biol *13*, 799-806. 10.1038/nchembio.2389.

Irannejad, R., Tomshine, J.C., Tomshine, J.R., Chevalier, M., Mahoney, J.P., Steyaert, J., Rasmussen, S.G., Sunahara, R.K., El-Samad, H., Huang, B., and von Zastrow, M. (2013). Conformational biosensors reveal GPCR signalling from endosomes. Nature *495*, 534-538. 10.1038/nature12000.

Irannejad, R., Tsvetanova, N.G., Lobingier, B.T., and von Zastrow, M. (2015). Effects of endocytosis on receptor-mediated signaling. Curr Opin Cell Biol *35*, 137-143. 10.1016/j.ceb.2015.05.005.

Irannejad, R., and von Zastrow, M. (2014). GPCR signaling along the endocytic pathway. Curr Opin Cell Biol *27*, 109-116. 10.1016/j.ceb.2013.10.003.

Janetzko, J., Kise, R., Barsi-Ryne, B., Siepe, D.H., Heydenreich, F.M., Masureel, M., Kawakami, K., Garcia, K.C., von Zastrow, M., Inoue, A., and Kobilka, B.K. (2021). Membrane phosphoinositides stabilize GPCR-arrestin complexes and offer temporal control of complex assembly and dynamics. bioRxiv, 2021.2010.2009.463790. 10.1101/2021.10.09.463790.

Jean-Charles, P.Y., Kaur, S., and Shenoy, S.K. (2017). G Protein-Coupled Receptor Signaling Through beta-Arrestin-Dependent Mechanisms. J Cardiovasc Pharmacol *70*, 142-158. 10.1097/FJC.0000000000000482.

Jensen, D.D., Lieu, T., Halls, M.L., Veldhuis, N.A., Imlach, W.L., Mai, Q.N., Poole, D.P., Quach, T., Aurelio, L., Conner, J., et al. (2017). Neurokinin 1 receptor signaling in endosomes mediates sustained nociception and is a viable therapeutic target for prolonged pain relief. Sci Transl Med *9*. 10.1126/scitranslmed.aal3447.

Jimenez-Vargas, N.N., Yu, Y., Jensen, D.D., Bok, D.D., Wisdom, M., Latorre, R., Lopez, C., Jaramillo-Polanco, J.O., Degro, C., Guzman-Rodriguez, M., et al. (2021). Agonist that activates the micro-opioid receptor in acidified microenvironments inhibits colitis pain without side effects. Gut. 10.1136/gutjnl-2021-324070.

Jirkof, P., Bratcher, N., Medina, L., Strasburg, D., Ebert, P., and Gaskill, B.N. (2020). The effect of group size, age and handling frequency on inter-male aggression in CD 1 mice. Sci Rep *10*, 2253. 10.1038/s41598-020-59012-4.

Johnston, C.A., Willard, F.S., Ramer, J.K., Blaesius, R., Roques, C.N., and Siderovski, D.P. (2008). State-selective binding peptides for heterotrimeric G-protein subunits: novel tools for investigating G-protein signaling dynamics. Comb Chem High Throughput Screen *11*, 370-381. 10.2174/138620708784534798.

Kamal, M., and Jockers, R. (2011). Biological Significance of GPCR Heteromerization in the Neuro-Endocrine System. Front Endocrinol (Lausanne) *2*, 2. 10.3389/fendo.2011.00002.

Karl, K., Paul, M.D., Pasquale, E.B., and Hristova, K. (2020). Ligand bias in receptor tyrosine kinase signaling. J Biol Chem *295*, 18494-18507. 10.1074/jbc.REV120.015190.

Khater, M., Wei, Z., Xu, X., Huang, W., Lokeshwar, B.L., Lambert, N.A., and Wu, G. (2021). G protein betagamma translocation to the Golgi apparatus activates MAPK via p110gamma-p101 heterodimers. J Biol Chem *296*, 100325. 10.1016/j.jbc.2021.100325.

Kotowski, S.J., Hopf, F.W., Seif, T., Bonci, A., and von Zastrow, M. (2011). Endocytosis promotes rapid dopaminergic signaling. Neuron *71*, 278-290. 10.1016/j.neuron.2011.05.036.

Kumari, P., Srivastava, A., Banerjee, R., Ghosh, E., Gupta, P., Ranjan, R., Chen, X., Gupta, B., Gupta, C., Jaiman, D., and Shukla, A.K. (2016). Functional competence of a partially engaged GPCR-beta-arrestin complex. Nat Commun *7*, 13416. 10.1038/ncomms13416.

Laporte, S.A., Oakley, R.H., Zhang, J., Holt, J.A., Ferguson, S.S., Caron, M.G., and Barak, L.S. (1999). The beta2-adrenergic receptor/betaarrestin complex recruits the clathrin adaptor AP-2 during endocytosis. Proc Natl Acad Sci U S A *96*, 3712-3717. 10.1073/pnas.96.7.3712.

Latorraca, N.R., Wang, J.K., Bauer, B., Townshend, R.J.L., Hollingsworth, S.A., Olivieri, J.E., Xu, H.E., Sommer, M.E., and Dror, R.O. (2018). Molecular mechanism of GPCR-mediated arrestin activation. Nature *557*, 452-456. 10.1038/s41586-018-0077-3.

Lee, M.H., Appleton, K.M., Strungs, E.G., Kwon, J.Y., Morinelli, T.A., Peterson, Y.K., Laporte, S.A., and Luttrell, L.M. (2016). The conformational signature of beta-arrestin2 predicts its trafficking and signalling functions. Nature *531*, 665-668. 10.1038/nature17154.

Lefkowitz, R.J., and Shenoy, S.K. (2005). Transduction of receptor signals by beta-arrestins. Science *308*, 512-517. 10.1126/science.1109237.

Luttrell, L.M., Wang, J., Plouffe, B., Smith, J.S., Yamani, L., Kaur, S., Jean-Charles, P.Y., Gauthier, C., Lee, M.H., Pani, B., et al. (2018). Manifold roles of beta-arrestins in GPCR signaling elucidated with siRNA and CRISPR/Cas9. Sci Signal *11*. 10.1126/scisignal.aat7650.

Mantovani, A. (1999). The chemokine system: redundancy for robust outputs. Immunol Today *20*, 254-257. 10.1016/s0167-5699(99)01469-3.

Masuho, I., Ostrovskaya, O., Kramer, G.M., Jones, C.D., Xie, K., and Martemyanov, K.A. (2015). Distinct profiles of functional discrimination among G proteins determine the actions of G protein-coupled receptors. Sci Signal *8*, ra123. 10.1126/scisignal.aab4068.

Maziarz, M., Park, J.C., Leyme, A., Marivin, A., Garcia-Lopez, A., Patel, P.P., and Garcia-Marcos, M. (2020a). Revealing the Activity of Trimeric G-proteins in Live Cells with a Versatile Biosensor Design. Cell *182*, 770-785 e716. 10.1016/j.cell.2020.06.020.

Maziarz, M., Park, J.C., Leyme, A., Marivin, A., Garcia-Lopez, A., Patel, P.P., and Garcia-Marcos, M. (2020b). Revealing the Activity of Trimeric G-proteins in Live Cells with a Versatile Biosensor Design. Cell *182*, 770-785.e716. 10.1016/j.cell.2020.06.020.

McCluskey, A., Daniel, J.A., Hadzic, G., Chau, N., Clayton, E.L., Mariana, A., Whiting, A., Gorgani, N.N., Lloyd, J., Quan, A., et al. (2013). Building a better dynasore: the dyngo compounds potently inhibit dynamin and endocytosis. Traffic *14*, 1272-1289. 10.1111/tra.12119.

McDonald, P.H., Cote, N.L., Lin, F.T., Premont, R.T., Pitcher, J.A., and Lefkowitz, R.J. (1999). Identification of NSF as a beta-arrestin1-binding protein. Implications for beta2-adrenergic receptor regulation. J Biol Chem *274*, 10677-10680. 10.1074/jbc.274.16.10677.

Meiser, A., Mueller, A., Wise, E.L., McDonagh, E.M., Petit, S.J., Saran, N., Clark, P.C., Williams, T.J., and Pease, J.E. (2008). The chemokine receptor CXCR3 is degraded following internalization and is replenished at the cell surface by de novo synthesis of receptor. J Immunol *180*, 6713-6724. 10.4049/jimmunol.180.10.6713.

Mikucki, M.E., Fisher, D.T., Matsuzaki, J., Skitzki, J.J., Gaulin, N.B., Muhitch, J.B., Ku, A.W., Frelinger, J.G., Odunsi, K., Gajewski, T.F., et al. (2015). Non-redundant requirement for CXCR3 signalling during tumoricidal T-cell trafficking across tumour vascular checkpoints. Nat Commun *6*, 7458. 10.1038/ncomms8458.

Mohammad Nezhady, M.A., Rivera, J.C., and Chemtob, S. (2020). Location Bias as Emerging Paradigm in GPCR Biology and Drug Discovery. iScience *23*, 101643. 10.1016/j.isci.2020.101643.

Musheshe, N., Schmidt, M., and Zaccolo, M. (2018). cAMP: From Long-Range Second Messenger to Nanodomain Signalling. Trends Pharmacol Sci *39*, 209-222. 10.1016/j.tips.2017.11.006.

Nakajima, C., Mukai, T., Yamaguchi, N., Morimoto, Y., Park, W.R., Iwasaki, M., Gao, P., Ono, S., Fujiwara, H., and Hamaoka, T. (2002). Induction of the chemokine receptor CXCR3 on TCR-stimulated T cells: dependence on the release from persistent TCR-triggering and requirement for IFN-gamma stimulation. Eur J Immunol *32*, 1792-1801. 10.1002/1521-4141(200206)32:6<1792::AID-IMMU1792>3.0.CO;2-0.

Nguyen, A.H., Thomsen, A.R.B., Cahill, T.J., 3rd, Huang, R., Huang, L.Y., Marcink, T., Clarke, O.B., Heissel, S., Masoudi, A., Ben-Hail, D., et al. (2019). Structure of an endosomal signaling GPCR-G protein-beta-arrestin megacomplex. Nat Struct Mol Biol *26*, 1123-1131. 10.1038/s41594-019-0330-y.

Oakley, R.H., Laporte, S.A., Holt, J.A., Caron, M.G., and Barak, L.S. (2000). Differential affinities of visual arrestin, beta arrestin1, and beta arrestin2 for G protein-coupled receptors delineate two major classes of receptors. J Biol Chem *275*, 17201-17210. 10.1074/jbc.M910348199.

Oldham, W.M., and Hamm, H.E. (2008). Heterotrimeric G protein activation by G-protein-coupled receptors. Nat Rev Mol Cell Biol *9*, 60-71. 10.1038/nrm2299.

Olsson, I.A.S., and Westlund, K. (2007). More than numbers matter: The effect of social factors on behaviour and welfare of laboratory rodents and non-human primates. Applied Animal Behaviour Science *103*, 229-254. https://doi.org/10.1016/j.applanim.2006.05.022.

Pack, T.F., Orlen, M.I., Ray, C., Peterson, S.M., and Caron, M.G. (2018). The dopamine D2 receptor can directly recruit and activate GRK2 without G protein activation. J Biol Chem *293*, 6161-6171. 10.1074/jbc.RA117.001300.

Pavlos, N.J., and Friedman, P.A. (2017). GPCR Signaling and Trafficking: The Long and Short of It. Trends Endocrinol Metab *28*, 213-226. 10.1016/j.tem.2016.10.007.

Peng, G.E., Pessino, V., Huang, B., and von Zastrow, M. (2021). Spatial decoding of endosomal cAMP signals by a metastable cytoplasmic PKA network. Nat Chem Biol *17*, 558-566. 10.1038/s41589-021-00747-0.

Rabin, R.L., Park, M.K., Liao, F., Swofford, R., Stephany, D., and Farber, J.M. (1999). Chemokine receptor responses on T cells are achieved through regulation of both receptor expression and signaling. J Immunol *162*, 3840-3850.

Rajagopal, S., Ahn, S., Rominger, D.H., Gowen-MacDonald, W., Lam, C.M., Dewire, S.M., Violin, J.D., and Lefkowitz, R.J. (2011). Quantifying ligand bias at seven-transmembrane receptors. Mol Pharmacol *80*, 367-377. 10.1124/mol.111.072801.

Rajagopal, S., Bassoni, D.L., Campbell, J.J., Gerard, N.P., Gerard, C., and Wehrman, T.S. (2013). Biased agonism as a mechanism for differential signaling by chemokine receptors. The Journal of biological chemistry *288*, 35039-35048. 10.1074/jbc.M113.479113.

Schmidt, E.V. (1999). The role of c-myc in cellular growth control. Oncogene *18*, 2988-2996. 10.1038/sj.onc.1202751.

Schneider, C.A., Rasband, W.S., and Eliceiri, K.W. (2012). NIH Image to ImageJ: 25 years of image analysis. Nat Methods *9*, 671-675. 10.1038/nmeth.2089.

Shukla, A.K., Manglik, A., Kruse, A.C., Xiao, K., Reis, R.I., Tseng, W.C., Staus, D.P., Hilger, D., Uysal, S., Huang, L.Y., et al. (2013). Structure of active beta-arrestin-1 bound to a G-protein-coupled receptor phosphopeptide. Nature *497*, 137-141. 10.1038/nature12120.

Smith, J.S., Alagesan, P., Desai, N.K., Pack, T.F., Wu, J.H., Inoue, A., Freedman, N.J., and Rajagopal, S. (2017). C-X-C Motif Chemokine Receptor 3 Splice Variants Differentially Activate Beta-Arrestins to Regulate Downstream Signaling Pathways. Molecular pharmacology *92*, 136-150. 10.1124/mol.117.108522.

Smith, J.S., Lefkowitz, R.J., and Rajagopal, S. (2018a). Biased signalling: from simple switches to allosteric microprocessors. Nat Rev Drug Discov *17*, 243-260. 10.1038/nrd.2017.229.

Smith, J.S., Nicholson, L.T., Suwanpradid, J., Glenn, R.A., Knape, N.M., Alagesan, P., Gundry, J.N., Wehrman, T.S., Atwater, A.R., Gunn, M.D., et al. (2018b). Biased agonists of the chemokine receptor CXCR3 differentially control chemotaxis and inflammation. Sci Signal *11*. 10.1126/scisignal.aaq1075.

Sriram, K., and Insel, P.A. (2018). G Protein-Coupled Receptors as Targets for Approved Drugs: How Many Targets and How Many Drugs? Mol Pharmacol *93*, 251-258. 10.1124/mol.117.111062.

Subramanian, A., Tamayo, P., Mootha, V.K., Mukherjee, S., Ebert, B.L., Gillette, M.A., Paulovich, A., Pomeroy, S.L., Golub, T.R., Lander, E.S., and Mesirov, J.P. (2005). Gene set enrichment analysis: a knowledge-based approach for interpreting genome-wide expression profiles. Proc Natl Acad Sci U S A *102*, 15545-15550. 10.1073/pnas.0506580102.

Thomsen, A.R.B., Jensen, D.D., Hicks, G.A., and Bunnett, N.W. (2018). Therapeutic Targeting of Endosomal G-Protein-Coupled Receptors. Trends Pharmacol Sci *39*, 879-891. 10.1016/j.tips.2018.08.003.

Thomsen, A.R.B., Plouffe, B., Cahill, T.J., 3rd, Shukla, A.K., Tarrasch, J.T., Dosey, A.M., Kahsai, A.W., Strachan, R.T., Pani, B., Mahoney, J.P., et al. (2016). GPCR-G Protein-beta-Arrestin Super-Complex Mediates Sustained G Protein Signaling. Cell *166*, 907-919. 10.1016/j.cell.2016.07.004.

Tsvetanova, N.G., Irannejad, R., and von Zastrow, M. (2015). G protein-coupled receptor (GPCR) signaling via heterotrimeric G proteins from endosomes. J Biol Chem *290*, 6689-6696. 10.1074/jbc.R114.617951.

Tsvetanova, N.G., and von Zastrow, M. (2014). Spatial encoding of cyclic AMP signaling specificity by GPCR endocytosis. Nat Chem Biol *10*, 1061-1065. 10.1038/nchembio.1665.

Whitmarsh, A.J., Shore, P., Sharrocks, A.D., and Davis, R.J. (1995). Integration of MAP kinase signal transduction pathways at the serum response element. Science *269*, 403-407. 10.1126/science.7618106.

Wootten, D., Christopoulos, A., Marti-Solano, M., Babu, M.M., and Sexton, P.M. (2018). Mechanisms of signalling and biased agonism in G protein-coupled receptors. Nat Rev Mol Cell Biol *19*, 638-653. 10.1038/s41580-018-0049-3.

Zalewska, M., Siara, M., and Sajewicz, W. (2014). G protein-coupled receptors: abnormalities in signal transmission, disease states and pharmacotherapy. Acta Pol Pharm *71*, 229-243.

Zhang, Y., Devries, M.E., and Skolnick, J. (2006). Structure modeling of all identified G protein-coupled receptors in the human genome. PLoS Comput Biol *2*, e13. 10.1371/journal.pcbi.0020013.

095

FIGURE 1

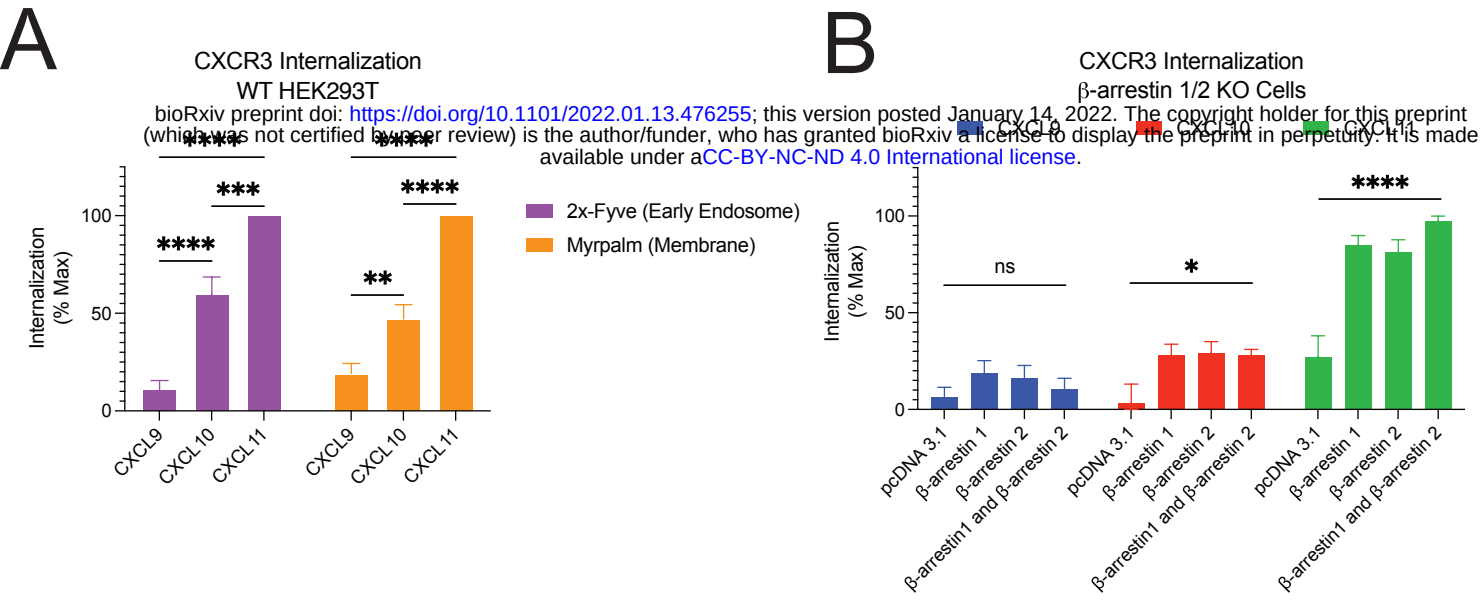

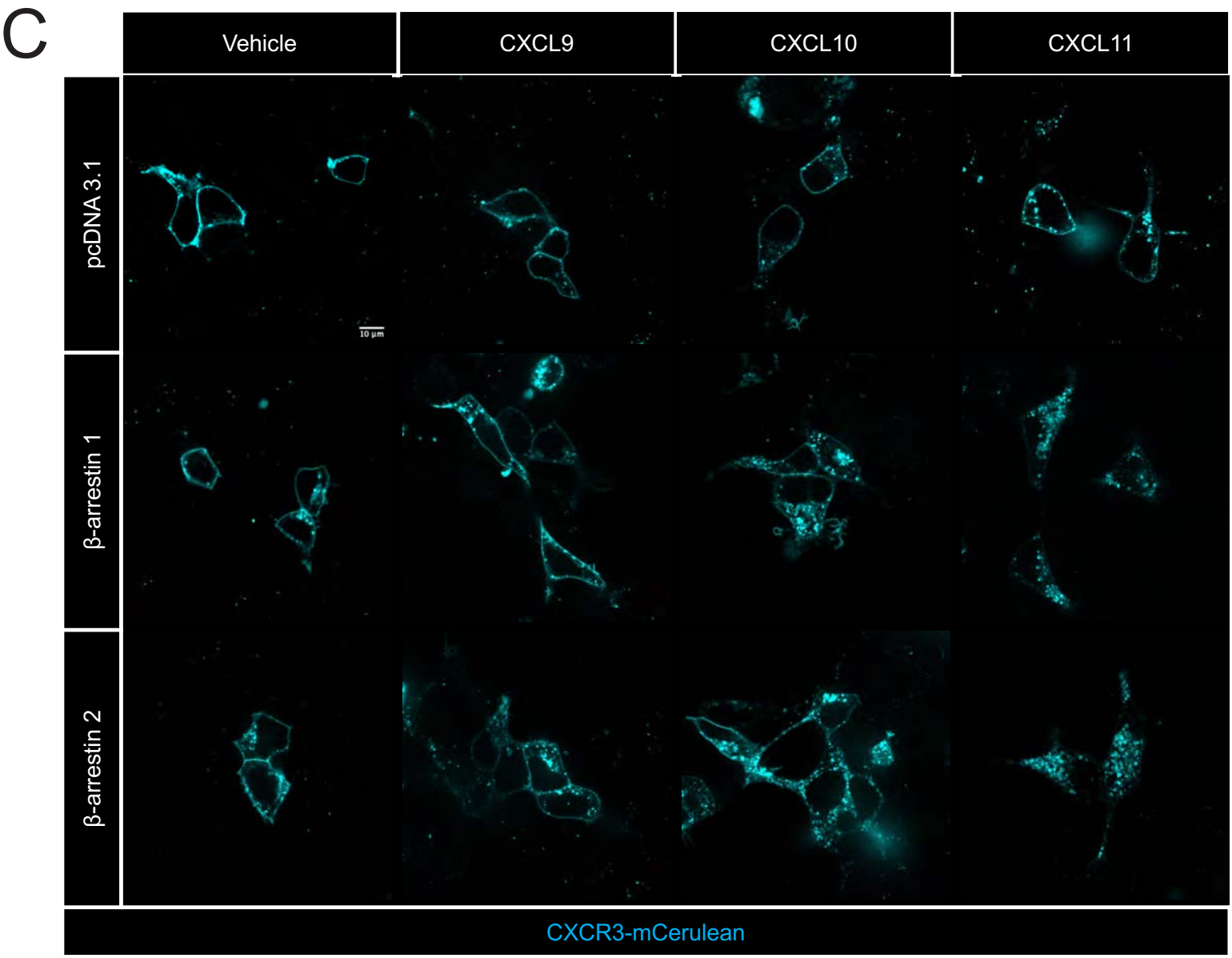

FIGURE 2

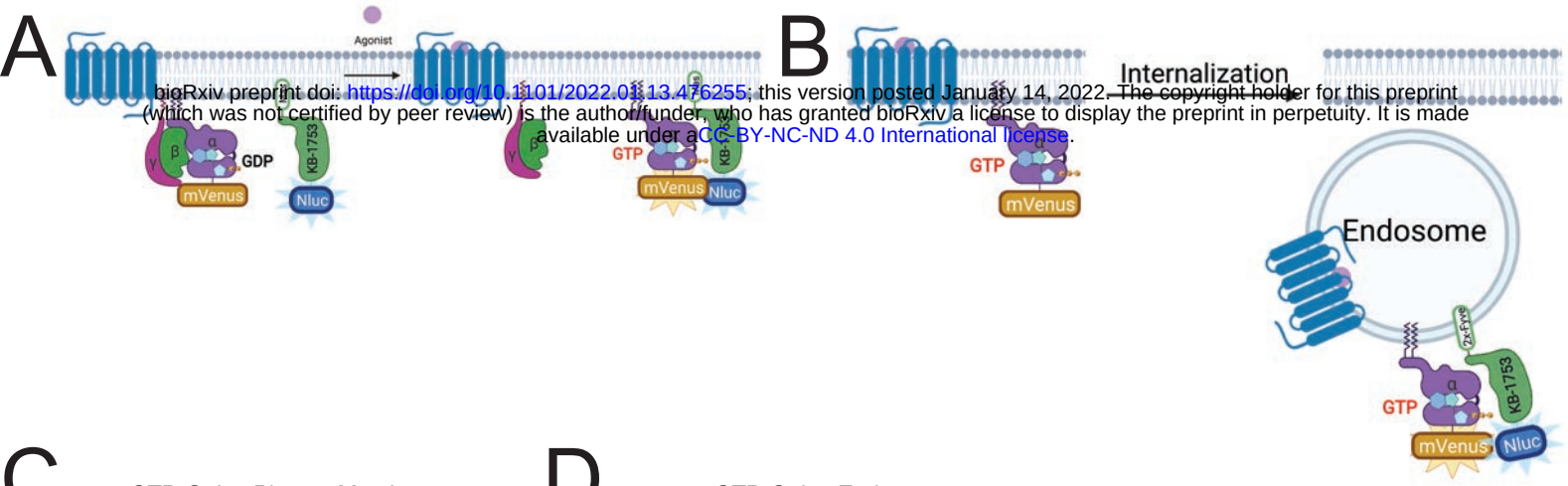

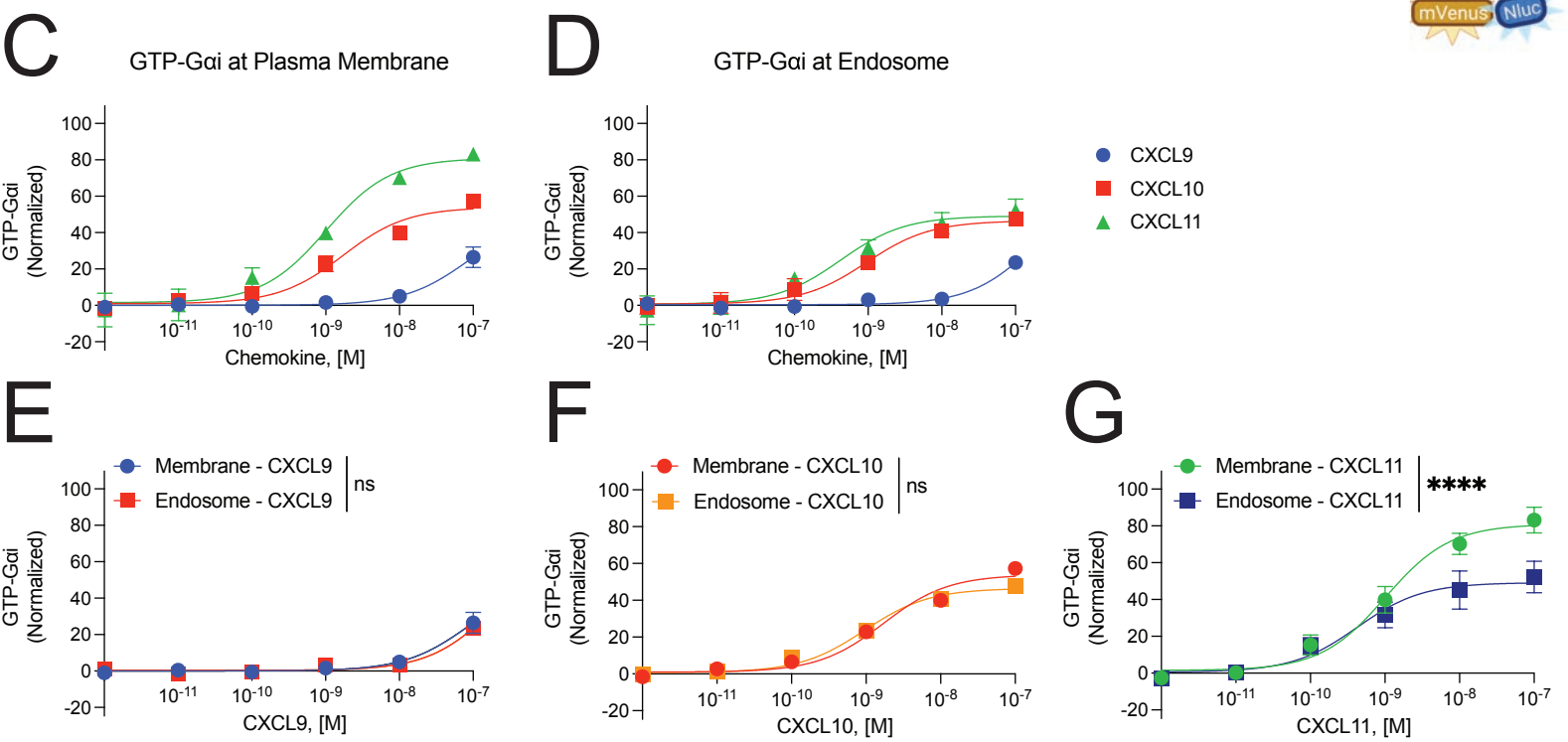

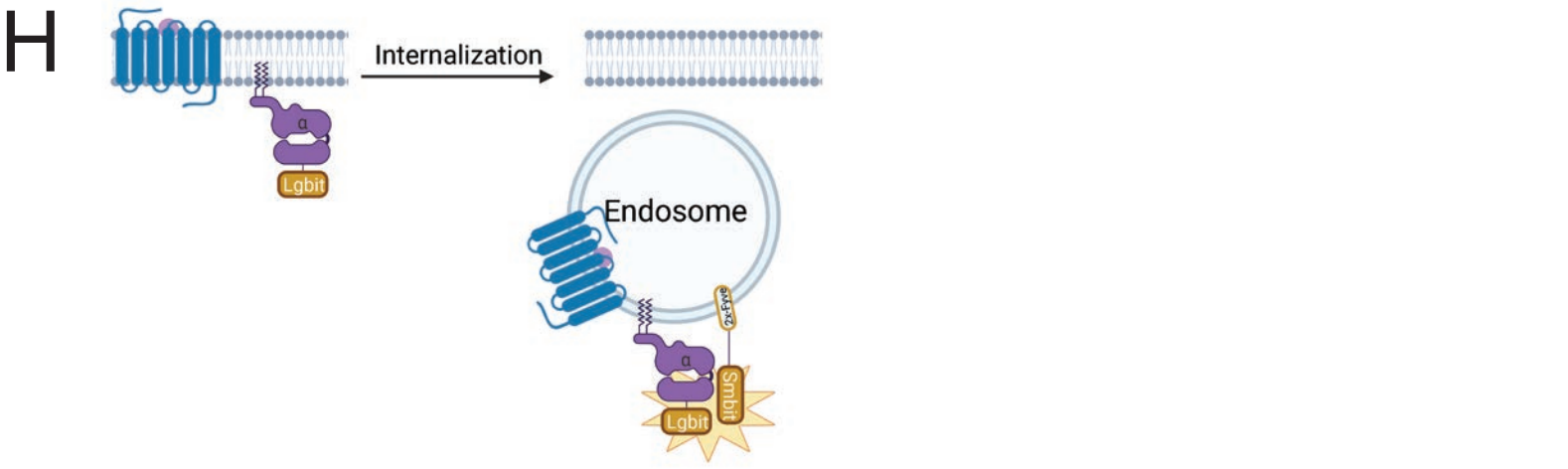

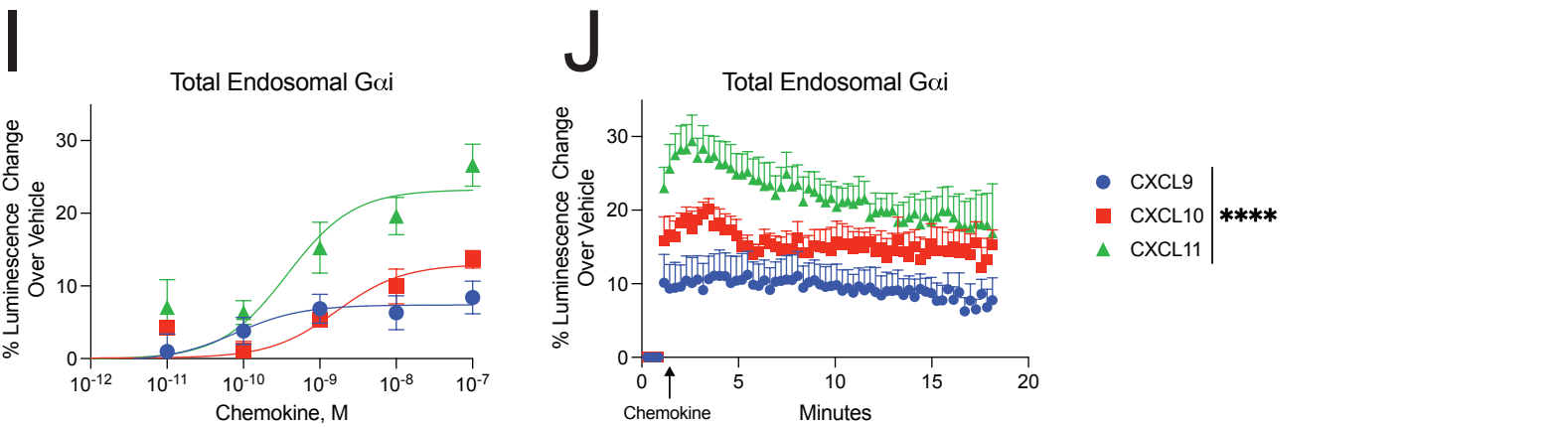

FIGURE 3

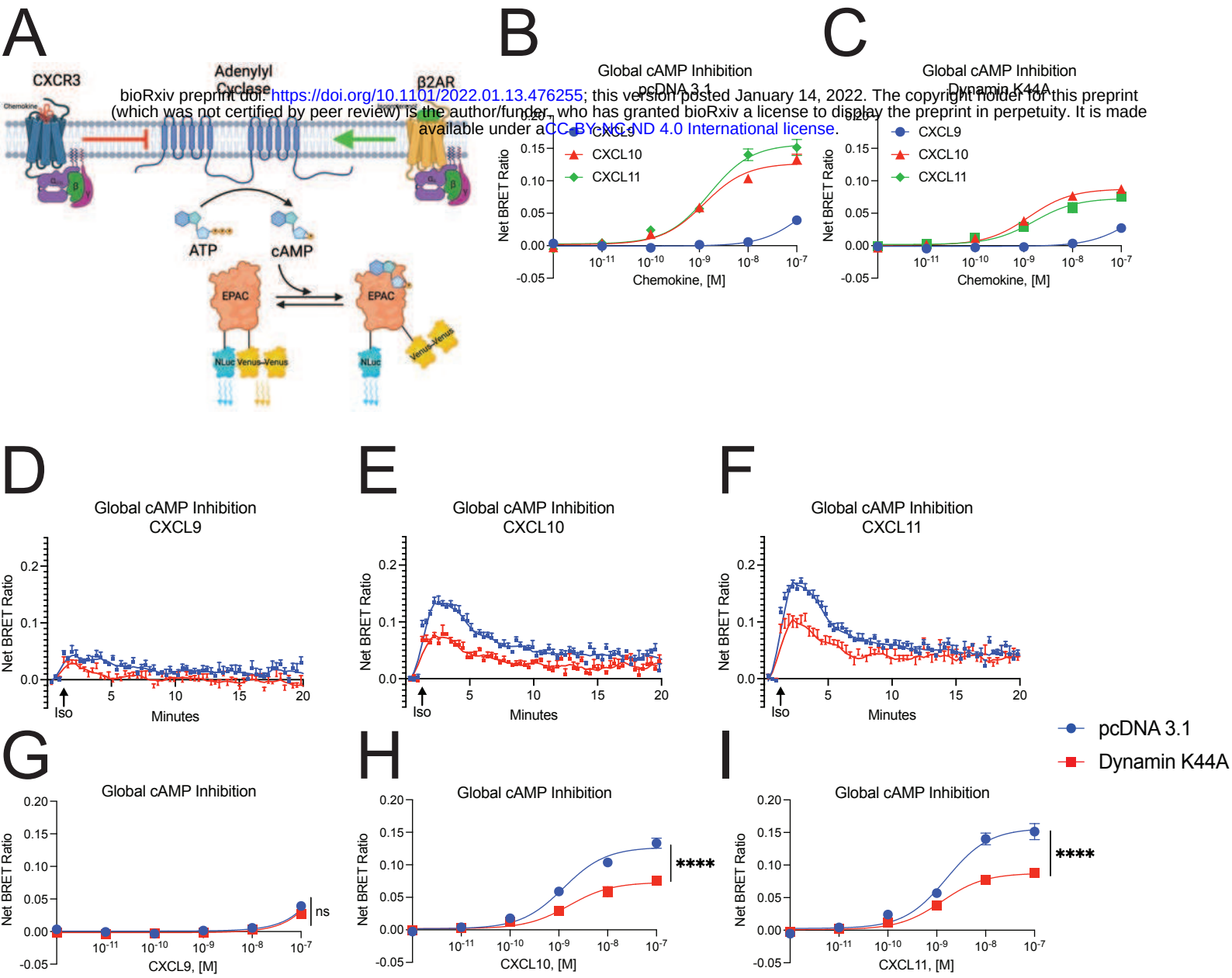

FIGURE 4

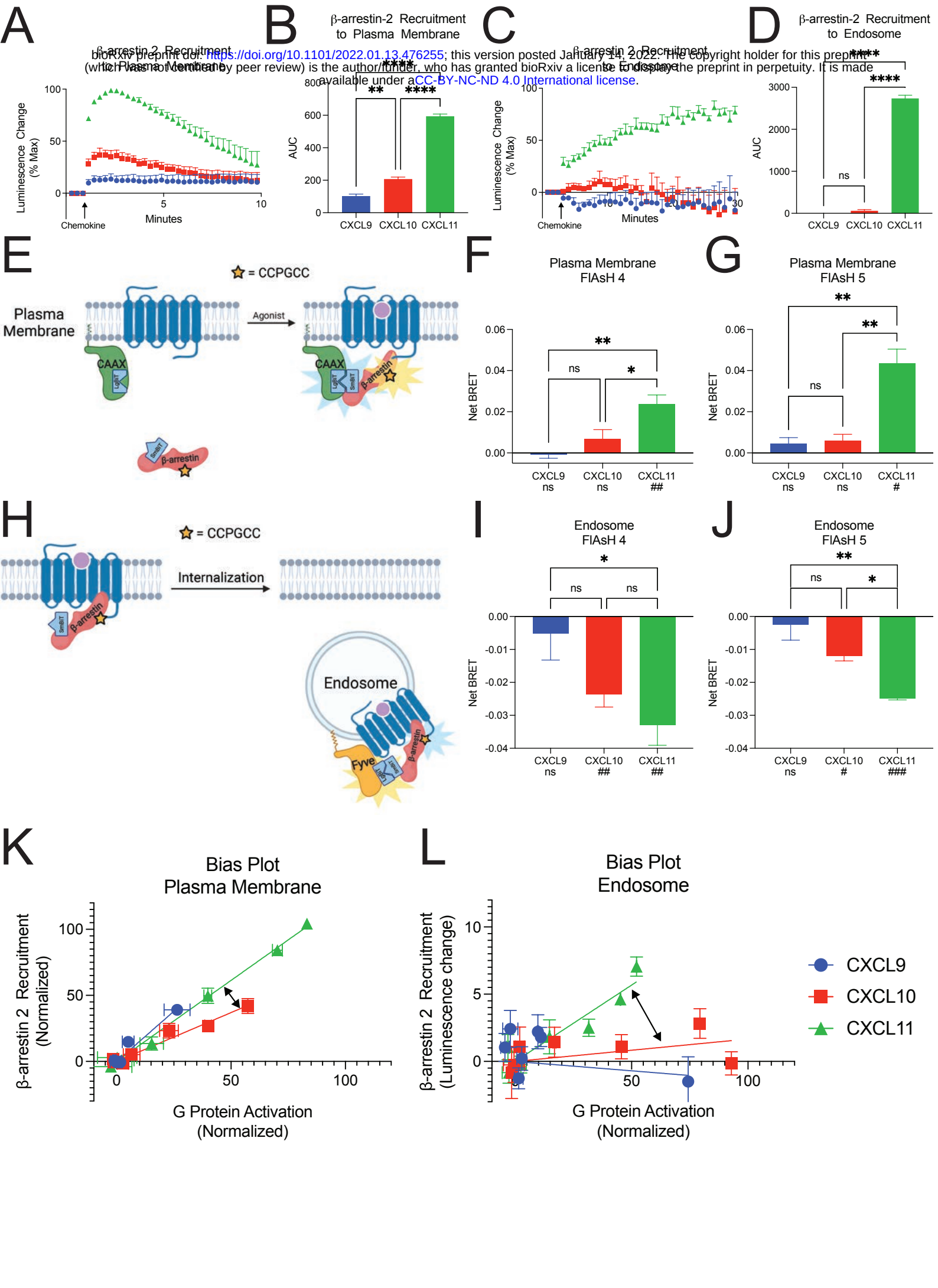

FIGURE 5

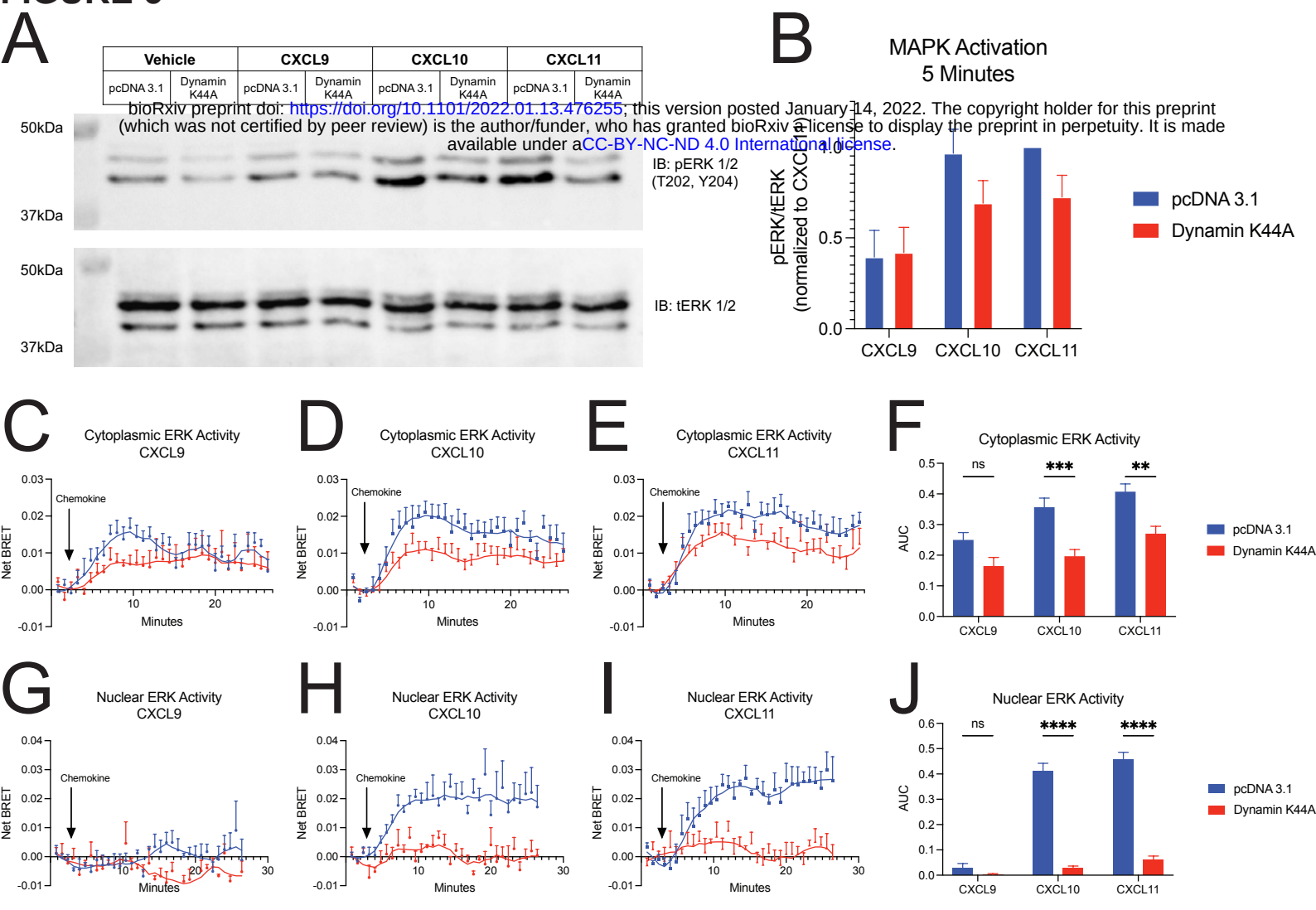

FIGURE 6

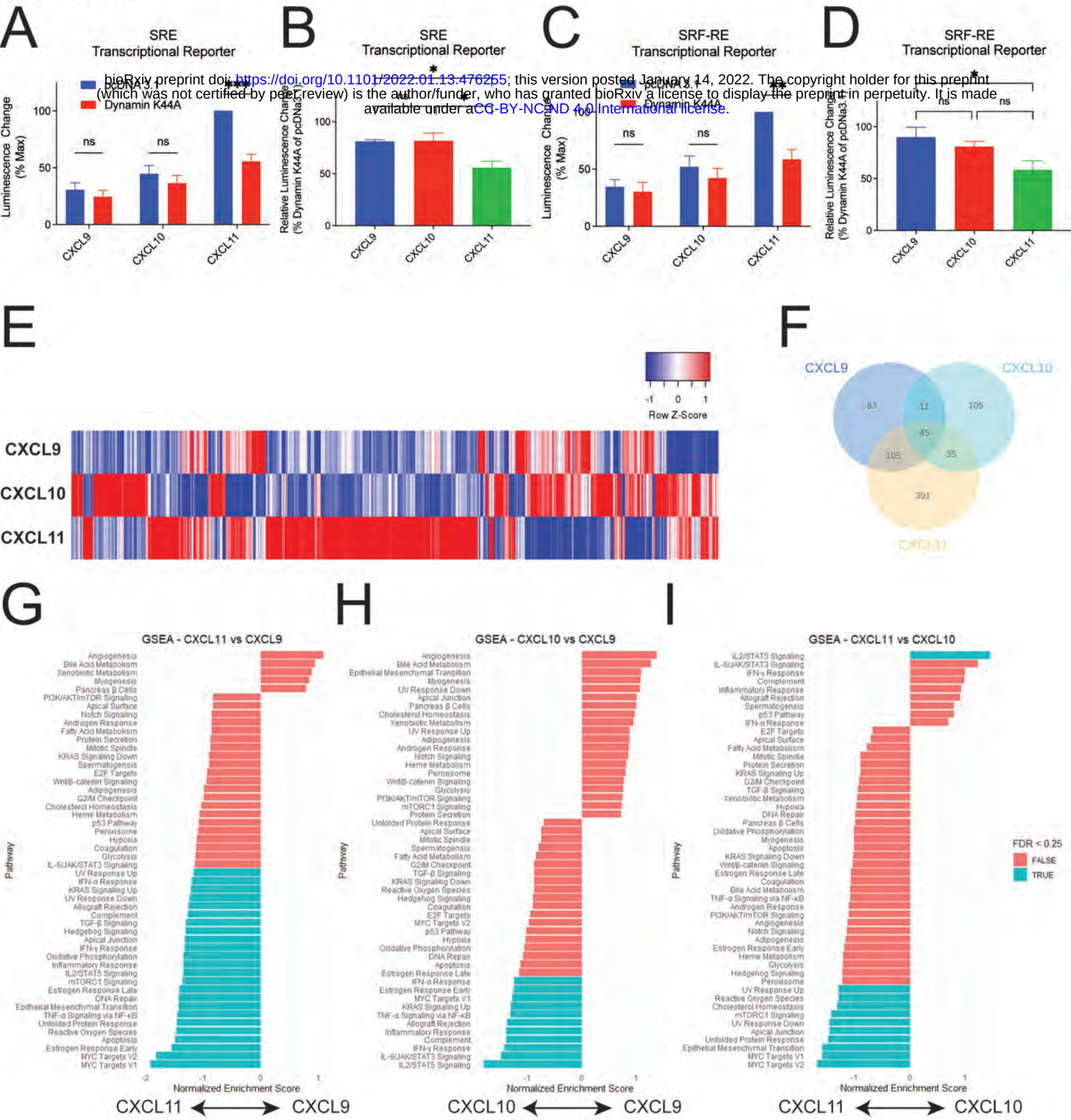

FIGURE 7

A

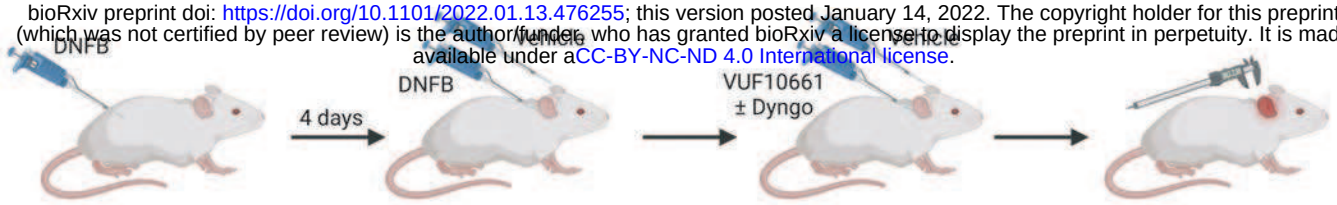

B

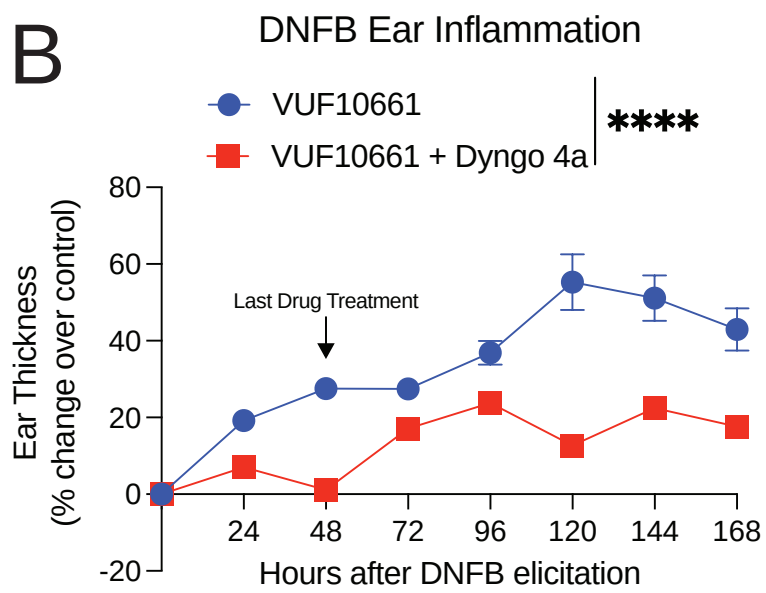

C